12-2022

Enhancing Human Schwann Cells Reparative Behavior using Heparin/Collagen Layer-by-layer Coatings

Luis Carlos Pinzon-Herrera
University of Arkansas, Fayetteville

Enhancing Human Schwann Cells Reparative Behavior using Heparin/Collagen Layer-by-layer Coatings

A dissertation submitted in partial fulfillment
of the requirements for the degree of
Doctor of Philosophy in Engineering with a concentration in Chemical Engineering

by

Luis Carlos Pinzon-Herrera
Universidad del Atlántico
Bachelor of Science in Chemistry, 2010

December 2022
University of Arkansas

This dissertation is approved for recommendation to the Graduate Council.

Jorge L. Almodovar-Montañez, Ph.D.
Dissertation Director

Shannon Servoss, Ph.D.
Committee Member

Audie Thompson, Ph.D.
Committee Member

Jeffrey Collins Wolchok, Ph.D.
Committee Member

Karthik Nayani, Ph.D.
Committee Member

ABSTRACT

When a peripheral nerve injury (PNI) occurs, the gold standard for tissue regeneration is the use of autografts. However, due to the secondary effects produced by multiple surgeries involved in the removal and implantation of autografts for very small lesions, it is possible to replace them with the use of Nerve Guide Conduits (NGCs). However, NGCs are limited to short lesions (less than 1 cm). This limitation is caused by the absence of compounds in the extracellular matrix (ECM) that autografts can provide. Since much of the regenerative process takes place on the NGC surface, our work aims to modify its surface using heparin and collagen coatings, two natural polymers present in the ECM. Heparin/collagen bilayers (HEP/COL) will increase biocompatibility, cell adhesion and migration, and allow the incorporation of neurotrophic factors such as Nerve Growth Factor (NGF). This research evaluates the effects on human Schwann cells (hSCs) when cultured on a commercial collagen NGC under four conditions: without coatings and with six heparin/collagen bilayers $(HEP/COL)_6$ with and without NGF supplemented to the culture medium (10 ng/ml). We have exhaustively characterized $(HEP/COL)_6$ coatings. The chemical structures of the polymers, the morphology, and the surface charge of the coatings could be determined. Real-time analysis of hSCs behavior showed three main phases: adhesion, proliferation, and adaptation. The adhesion phase was increased in the conditions with $(HEP/COL)_6$, and the viability studies showed an increase of up to 250% compared to cells grown on polystyrene without coatings. The cell morphology has never been altered by $(HEP/COL)_6$, as well as the morphology of the coated NGC. Cell migration was favored, and $(HEP/COL)_6$ also increased the expression of some proteins such as BDNF, which promotes the duration of the myelination process, or TNF alpha, which is a mediator of inflammatory and immune functions. Concerning the surface modification of a commercial NGC, these studies showed an increase of more than 200% in cell viability when compared to uncoated NGCs. We also determined the presence of heparin and evidenced the cell adhesion on $(HEP/COL)_6$ coated NGCs. In conclusion, $(HEP/COL)_6$ seems to be a promising strategy to improve the performance of NGCs.

DEDICATION

I dedicate this thesis to my beautiful wife and son, Anllely and Alejandro, for all your unconditional love and support; you are the engine of my life. I love you! To my dear mother, Onit Herrera, for trusting me and always supporting me in all my projects. I love you, mother! To my handsome sisters, Pao, Sari, and Patry. And to the memory of my beloved father, Luis Carlos Pinzon Torres, who supported me in achieving this doctorate. I miss you every day, and I miss you more than words can say. Thank you, father, for believing in my dream!

TABLE OF CONTENTS

List of Publications

- Chapter one

Portions of chapter one were previously published as:

1) Ayala-Caminero, R., **Pinzon-Herrera, L.,** Rivera, C.A., & Almodovar, J. (2017). Polymeric scaffolds for three-dimensional culture of nerve cells: a model of peripheral nerve regeneration. *MRS communications*, 7, 391-415. Published. Copyright©, Reprinted with permission.

2) Castilla-Casadiego, D. A., **Pinzon-Herrera, L.,** Perez-Perez, M., Quiñones-Colón, B. A., Suleiman, D., & Almodovar, J. (2018). Simultaneous characterization of physical, chemical, and thermal properties of polymeric multilayers using infrared spectroscopic ellipsometry. *Colloids and Surfaces A: Physicochemical and Engineering Aspects*, *553*, 155-168. Published. Copyright© 2018, Reprinted with permission from Elsevier.

- Chapter two is:

1) **Pinzon-Herrera, L.,** Mendez-Vega, J., Mulero-Russe, A., Castilla-Casadiego, D. A., & Almodovar, J. (2020). Real-time monitoring of human Schwann cells on heparin-collagen coatings reveals enhanced adhesion and growth factor response. *Journal of Materials Chemistry B*, *8*, 8809-8819. Published. Reproduced with permission from the Royal Society of Chemistry.

- Chapter three is:

1) **Pinzon-Herrera, L.,** Magness, J., Apocada-Reyes, H., Sanchez, J., & Almodovar, J. (2022). Heparin-collagen layer-by-layer coatings improve protein expression potential and cell migration in human Schwann cells: stability studies and application to a commercial Nerve guide conduit. *Pending Publication*.

INTRODUCTION

Peripheral nerve injury (PNI) is a lesion that causes damage to peripheral nerve tissue and prevents nerve function.[1] Therefore, if the PNI severity involves a complete nerve rupture, self-regeneration is impossible, and a surgical process is necessary to repair the tissue.[1,2] More than 500,000 surgeries caused by PNIs are reported annually in the United States.[3,4] In these cases, the most standardized procedure is autograft implantation.[5] However, despite its significant advantages, the use of autografts implies the possibility that the patient suffers some adverse side effects such as the appearance of scars, loss of function of the donor site, infections, or additional surgeries.[3,6,7] As a result, nerve guide conduits (NGCs) have recently been studied as potential substitutes for autografts.[2] Nevertheless, the challenge is to repair larger lesions because, due to the lack of components in the extracellular matrix (ECM), NGCs are limited to short lesions of no more than 1 cm.[2]

Accompaniment with growth factors (GFs) is vital to promote neuronal regeneration when NGCs are used.[5] However, inefficient methods of dosing GFs result in unintended negative effects [8] Tissue engineering is advancing in studying and developing biodegradable devices containing growth factors.[9] Once implemented, their primary function is to release GFs in a controlled way.[10] The challenge is to improve the performance, biocompatibility, and functionalization of GFs to NGCs. A simple but effective method to modify the surface of implants is the production of polyelectrolyte multilayers through the Layer-by-layer (LbL) method.[11] The LbL technique uses electrostatic interactions between polymers by alternating a polycation to a polyanion to create stable multilayers. Polyelectrolyte coatings on substrate surfaces are gaining wide attention from the scientific community. When polymers of a biological character are used, their properties can be manipulated to bind growth factors and promote their stabilization and delivery.[12]

Our group has worked hard by combining heparin (HEP) and collagen (COL) polymers to create multilayers and in vitro assays with different types of cells.[13–17] This research mainly uses six bilayers HEP/COL or what will be the same (HEP/COL)6. The choice of HEP/COL lies primarily in two critical factors, their properties as biopolymers and their difference in electrical charge, negative for HEP and positive for COL.[13–15] Briefly, HEP is present in the ECM, has a strong negative charge and high GFs affinity, drives axon growth during regeneration processes, and is widely known as an anticoagulant agent.[18] On the other hand, COL is a protein commonly found in many tissues and is known as one of the leading providers of support to the ECM; therefore, its use will decrease the immune response.[19] For this research, our experimental design also focus on *in vitro* tests on a Collagen-based NGC approved by the FDA since this type of implant is ideal for promoting nerve tissue regeneration and generating a low immune response.[19]

The neuron is the fundamental unit of the nervous system and, therefore, of the peripheral nerve. In some nerve fibers, the axons of neurons are surrounded by Schwann cells, which produce a compound called myelin, thereby creating a layer along the length of the axon called the myelin sheath. The function of myelin is to increase the speed of communication between neurons.[20] SCs play an essential role in peripheral nerve regeneration since they not only produce myelin, but once PNI occurs, they execute a package of functions in a way known as *"Repair Schwann cells."* Among these functions are sending survival signals, producing GFs, activating the immune response, and facilitating the action of macrophages.[15,21,22] Therefore, it is vital to improving the abilities of SCs, such as the adhesion, migration, protein expression, and other factors involved in peripheral nerve tissue repair.

This thesis focuses on three main objectives: (1) the use of the layer-by-layer method to deposit $(HEP/COL)_6$ on different surfaces, including a commercial collagen-based NGC, a complete characterization of the coatings, and some stability tests; (2) *in vitro* studies of $(HEP/COL)_6$ on tissue culture polystyrene (TCPS), including studies of proliferation, adhesion, viability, migration, extension, and protein expression potential by SCs; and (3) the modification of the surface of an NGC with the use of $(HEP/COL)_6$ and some *in vitro* assays to study the response of the SCs.

References

[1] S.J. Bunn, CHARACTERIZATION OF SCHWANN CELLS STIMULATED BY DC ELECTRIC FIELDS, 2019.

[2] B. Pfister, T. Gordon, J.R. Loverde, A.S. Kochar, S.E. Mackinnon, D.K. Cullen, Biomedical Engineering Strategies for Peripheral Nerve Repair: Surgical Applications, State of the Art, and Future Challenges, Crit Rev Biomed Eng. 39 (2011) 81–124. https://doi.org/10.1615/CritRevBiomedEng.v39.i2.20.

[3] L. Tian, M.P. Prabhakaran, S. Ramakrishna, Strategies for regeneration of components of nervous system: scaffolds, cells and biomolecules, Regen Biomater. 2 (2015) 31–45. https://doi.org/10.1093/rb/rbu017.

[4] K. Brattain, Analysis of the peripheral nerve repair market in the United States, (2013) 1–11. https://www.semanticscholar.org/paper/ANALYSIS-OF-THE-PERIPHERAL-NERVE-REPAIR-MARKET-IN-Brattain/cba129fbda15780ea0abd09da3da97de04f9c6b5 (accessed February 13, 2022).

[5] C.E. Schmidt, J.B. Leach, Neural Tissue Engineering: Strategies for Repair and Regeneration, Annu Rev Biomed Eng. 5 (2003) 293–347. https://doi.org/10.1146/annurev.bioeng.5.011303.120731.

[6] S. Madduri, B. Gander, Schwann cell delivery of neurotrophic factors for peripheral nerve regeneration, Journal of the Peripheral Nervous System. 15 (2010) 93–103. https://doi.org/10.1111/j.1529-8027.2010.00257.x.

[7] S. Ho, P. Labroo, K.M. Lin, S. Himanshu, J. Shea, B. Gale, J. Agarwal, Designing a Novel Drug Delivering Nerve Guide: A Preliminary Study, J Med Biol Eng. 39 (2019) 294–304. https://doi.org/10.1007/s40846-018-0393-y.

[8] L. Aloe, M.L. Rocco, P. Bianchi, L. Manni, Nerve growth factor: From the early discoveries to the potential clinical use, J Transl Med. 10 (2012) 1–15. https://doi.org/10.1186/1479-5876-10-239.

[9] J.E. Babensee, L. v Mcintire, A.G. Mikos, Growth Factor Delivery for Tissue Engineering, 2000.

[10] H. Lo, S. Kadiyala, ; S E Guggino, K.W. Leong3, Poly(L-lactic acid) foams with cell seeding and controlled-release capacity, n.d.

[11] J. Almodóvar, R. Guillot, C. Monge, J. Vollaire, S. Selimovíc, J.L. Coll, A. Khademhosseini, C. Picart, Spatial patterning of BMP-2 and BMP-7 on biopolymeric films and the guidance of muscle cell fate, Biomaterials. 35 (2014) 3975–3985. https://doi.org/10.1016/j.biomaterials.2014.01.012.

[12] J. Almodóvar, L.W. Place, J. Gogolski, K. Erickson, M.J. Kipper, Layer-by-layer assembly of polysaccharide-based polyelectrolyte multilayers: a spectroscopic study of hydrophilicity, composition, and ion pairing, Biomacromolecules. 12 (2011) 2755–2765. https://doi.org/10.1021/bm200519y.

[13] D. Castilla-Casadiego, J. Garcia, A.J. Garcia, J. Almodóvar, Heparin/Collagen Coatings Improve Human Mesenchymal Stromal Cell Response to Interferon Gamma, ACS Biomater Sci Eng. 5 (2019) 2793–2803.

[14] D.A. Castilla-Casadiego, L. Pinzon-Herrera, M. Perez-Perez, B.A. Quiñones-Colón, D. Suleiman, J. Almodovar, Simultaneous characterization of physical, chemical, and thermal properties of polymeric multilayers using infrared spectroscopic ellipsometry, Colloids and Surfaces A. 553 (2018) 155–168. https://doi.org/10.1016/j.colsurfa.2018.05.052.

[15] L. Pinzon-Herrera, J. Mendez-Vega, A. Mulero-Russe, D.A. Castilla-Casadiego, J. Almodovar, Real-time monitoring of human Schwann cells on heparin-collagen coatings reveals enhanced adhesion and growth factor response, J Mater Chem B. 8 (2020) 8809–8819. https://doi.org/10.1039/d0tb01454k.

[16] M. Haseli, D.A. Castilla-Casadiego, L. Pinzon-Herrera, A. Hillsley, K.A. Miranda-Munoz, S. Sivaraman, A.M. Rosales, R.R. Rao, J. Almodovar, Immunomodulatory functions of human mesenchymal stromal cells are enhanced when cultured on HEP/COL multilayers supplemented with interferon-gamma, Mater Today Bio. 13 (2022). https://doi.org/10.1016/j.mtbio.2021.100194.

[17] S.J. Cifuentes, P. Priyadarshani, D.A. Castilla-Casadiego, L.J. Mortensen, J. Almodóvar, M. Domenech, Heparin/collagen surface coatings modulate the growth, secretome, and morphology of human mesenchymal stromal cell response to interferon-gamma, J Biomed Mater Res A. 109 (2021) 951–965. https://doi.org/10.1002/jbm.a.37085.

[18] K. Zhang, D. Huang, Z. Yan, C. Wang, Heparin/collagen encapsulating nerve growth factor multilayers coated aligned PLLA nanofibrous scaffolds for nerve tissue engineering, J Biomed Mater Res A. 105A (2017) 1900–1910. https://doi.org/10.1002/jbm.a.36053.

[19] R. Ayala-caminero, L. Pinzón-herrera, C.A. Rivera Martinez, J. Almodovar, Polymeric scaffolds for three-dimensional culture of nerve cells: a model of peripheral nerve regeneration, MRS Commun. 7 (2017) 391–415. https://doi.org/10.1557/mrc.2017.90.

[20] G.J. Siegel, R. Wayne Albers, S.T. Brady, D.L. Price, Basic Neurochemistry: Molecular, cellular, and medical aspects, 7th ed., Elsevier Academic Press, 2006. http://elsevier.com.

[21] C. Cheng, D.W. Zochodne, In vivo proliferation, migration and phenotypic changes of Schwann cells in the presence of myelinated fibers, Neuroscience. 115 (2002) 321–329. https://doi.org/10.1016/s0306-4522(02)00291-9.

[22] K.R. Jessen, R. Mirsky, The repair Schwann cell and its function in regenerating, J Physiol. 594 (2016) 3521–3531. https://doi.org/10.1113/JP270874.

CHAPTER 1. LITERATURE REVIEW

1.1 Peripheral Nerve Regeneration

The nervous system is the platform that communicates, transfers, and integrates the details for regulation and control of each of their biologic actions, reactions, and intermediate events. This occurs via a dedicated set of cells (e.g., neurons and glial cells) that together constitute the neuron fibers, fascicles, nerve ramifications, and overall nervous system that interconnects everything in the body. A nerve may be damaged due to severe nerve injury (neurotmesis or axonotmesis) [1] or neurodegenerative diseases (peripheral neuropathy),[2] both requiring medical intervention. Currently, healing and recovery of the nerves' fundamental performance remains limited: even with a successful nerve reconstruction resulting from an autologous nerve transplantation. Autologous nerve transplantation is the first line therapy (the "gold standard") as it is ready to address complicated nerve gaps resulting from a serious wound. It is non-immunogenic and provides an immediate nerve bridge that contains viable Schwann cells (SCs) and crucial signaling molecules involved in axonal renewal. However, there are multiple limitations in the use of autografts, including the potential need for a second surgery, the scar and/or neuroma formation, the inferiority against the original nerve, and functional loss (only 51.6% may gain a motor recovery, and 42.6% may obtain sensory healing).[3–5]

In the USA, damage to the nervous system is impacting approximately 20 million people,[4] and implicates around US $150 billion in annual healthcare expenses.[5] Therefore, significant efforts and resources for the studies of nerve regeneration strategies have been invested, including a deep fundamental understanding of the regeneration process using cellular models. Platforms for 3D cell culture have been developed to mimic the native peripheral nerve system (PNS) cell growth and function, in order to study tissue repair or diseases of the nervous system (e.g., Parkinson and Alzheimer).[6–8] There is a need to introduce better approaches for therapeutic

nerve regeneration. 3D cell culture models provide a practical and empirical way of observing cell activity and enable the quantification of the possible outcomes under different controlled conditions. The properties and functions of every cell in a distinct body are already encoded within the cells, at a level of detail that organizes and supports the complete sequence of biologic events for the development of cells to their mature stage with a specific role.[9] In the case of a damaged cell and/or tissue, it is expected that with the appropriate conditions the cells will activate and respond to specific signals to perform their role in the reconstruction and regeneration of damaged tissue.[10,11]

Experimental strategies are focused on modeling the ideal settings to provide the appropriate environment for neurons in an effort to restore a level of performance comparable prior with any injury. Research in regenerative medicine and tissue engineering uses a variety of polymeric devices to offer a suitable 3D cellular arrangement that supports neuronal growth and maturation to produce modern healthcare alternatives.[12] 3D cell culture models will precede in vivo developments. The general approaches for 3D cellular models are relevant as they are closer to in vivo systems and enable a more profound perspective of the cell development and fate characteristics (e.g., via imaging, molecular biology and genomics/transcriptomics techniques, and other analytical techniques); thus, ensuring the proposed designs, treatments, and potential benefits are well understood before any test subject is exposed to measured risks, or otherwise unwanted effects.[8]

1.2 Selection of cells for in vitro models

The use of in vitro cellular models have advantageous features over in vivo models, particularly those aspects regarding technical complexity, costs, and ethical concerns.[13] The appropriate selection of cells for the in vitro cellular models will support projections and expectations for

potential in vivo models. Moreover, in vitro cellular models are not necessarily subjected to regulations as with animal or human models. The goal is to obtain representation of the subject tissues and translate the research towards clinical developments. Yet, the biological characterizations made at the laboratory barely exemplifies what is to be expected in normal conditions, regardless of the source. For this, researchers can use primary cells (cells isolated directly from human or animal tissue), or cell lines (cells that have been continually passaged over a long period of time). Cell lines are cost-effective option but may be less physiologically representative of native cells because cell lines have been immortalized. Primary cells may be more representative of the native tissue; however, they need to be isolated from animals leading to increased oversight. Within the PNS, there is increased accessibility to obtain primary cells, such as SCs from sciatic nerve and neurons or mixed cultures from dissociated or whole dorsal root ganglia (DRG), compared to CNS cells that typically need to undergo several cell-specific purification steps. Researchers should select their test subjects strategically considering the resources available, and in a step wise approach per the progress obtained, and future developments envisioned.

1.3 Peripheral Nerve Biology

There are two (2) areas defining the nervous system, the central nervous system (CNS) consisting of the brain and the spinal cord; and the PNS, which is distributed along a large network of neurons connected to the tissues, organs, and anatomical systems in the body that sustain life. The nervous system is the channel for inputs and outputs (stimulus and a response) that enables organisms to become aware of their environment. The nervous system manages all the actions in a body, either voluntary or involuntarily. For this, different types of neurons are continuously active: the afferent neurons, which obtain information from the five senses, and pass it to the CNS; the multipolar interneurons, which relay messages between other neurons within the CNS;

and the efferent neurons, which drive our motor skills via the PNS. If a patient suffers an efferent fiber injury, they may not be able to move the innervated tissue because the brain impulse would not relay to the muscle. Likewise, if the impairment happens in an afferent fiber, the brain will not sense stimulus within the environment. As nerves carry both types of neuron fibers, a combination of efferent and afferent fibers are affected by injury. There are many levels of complexity among voluntary and involuntary reactions that are made possible by the nervous system. Identifying a situation, deciding what to do next, and performing an action is an example of the communication of the brain and the body, and the velocity of this process will vary on other factors not in the scope of this discussion. However, there are some "closed loops" where afferent fibers are directly connected to efferent fibers, and an impulse does not necessarily reach the brain (e.g., reflexes, equilibrium, and other involuntary actions).

Nerves are formed as a cascade of conduits inside other conduits.[14] The nerve is surrounded by a protective tissue known as the epineurium. Inside of it are the blood vessels and neuron bundles along with conduits called fascicles. As illustrated in **Figure 1-1**, the neurons can carry impulses or action potentials to the soma, then propagate the signals along the axon and axon terminals. The axons are protected by a myelin sheath produced by SCs located within the endoneurium. Early regeneration of the axon is what prompts the restitution of the nerve function.[15] There is some regenerative ability in the nervous system,[16] and this is true specifically in the PNS as it is exposed to macrophages that clear damaged tissue; and later assisted by SCs, which guide axon regeneration and provide the myelin sheath to support the re-connection between any gap.[17]

The PNS nerves branches out of the CNS to sense and collect input signals, and it is also responsible for transmitting the commands that controls muscle movement. The biochemical explanation of neuronal impulses, also known as potential actions, is described as an electro-chemical wave propagated within the surface membrane of a neuron. The initial stimulation of

neuron opens channels leading to sodium (Na^+) influx that depolarizes the membrane. The signal propagates as the adjacent section of membrane allows Na+ influx and depolarization. This wave of depolarization continues at a rapid rate down the neuron, resulting in a nerve impulse traveling inbound (afferent, sensory) and outbound (efferent, motor) to or from the brain in milliseconds.[14]

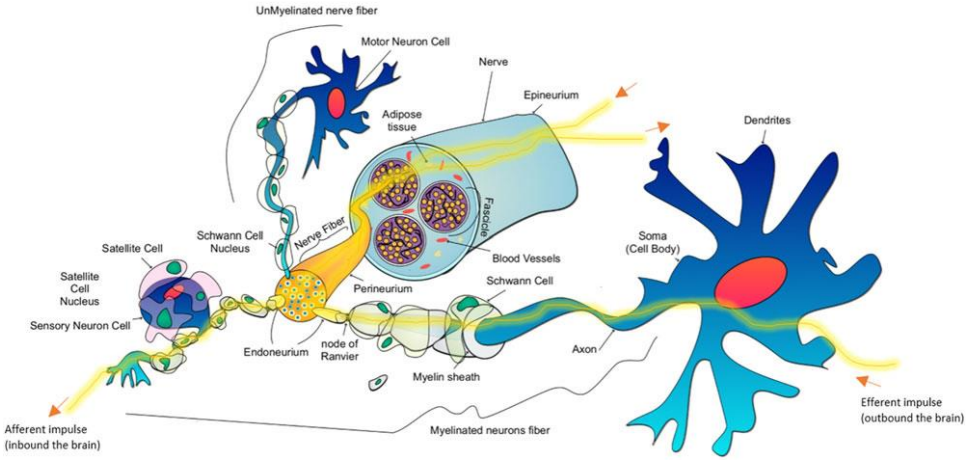

Figure 1-1. Basic structure of a nerve. From *Polymeric scaffolds for three-dimensional culture of nerve cells: a model of peripheral nerve regeneration*. Copyright©, Reprinted with permission.

After a severe nerve injury, the axon separates from the soma and, cytokines/GFs surrounding the injury will recruit and activate macrophages, which then infiltrate the site of injury to clean-up axon and myelin debris – this is known as Wallerian degeneration.[18,19] Wallerian degeneration is a controlled phase that extends to the following node of Ranvier, which is a gap in the myelin sheath that is exposed to the ECM. Wallerian degeneration stops the synapse and communication between the neural networks leading to atrophy of the associated muscle or gland, which could become permanently deteriorated if the axon fails to re-establish connectivity.

The neuron gap is defined as two parts: the proximal stump closest to the soma and distal stump that will degenerate. After macrophages remove the degenerated debris, the soma grows as the nucleus migrates towards the cell boundaries, and the local non-myelinating SCs at the

endoneurium align to guide axon regeneration. A regenerated axon sprouts from the proximal end and grows to join the two ends to reestablish the network connection. To ensure the proper reconnection, surgery helps to establish a guide for these sprouts leading to eventual re-innervation, either by using autologous nerve transplant or an engineered scaffold.

During nerve regeneration, the native ECM must be reconstructed. The major components of the ECM in the nervous system can be divided in four (4) groups: collagens and related molecules as structural parts (e.g., Types I, II, III, IV, and V); non-collagenous glycoproteins as binding agents of cells to mediate their effects or induce cell binding to other molecules (e.g., laminin (LN), fibronectin, entactin, and vitronectin.); glycosaminoglycans (GAGs) to facilitate cell migration, adhesion, and organization, as well as support the formation of proteoglycans by providing the chains of several functional groups (e.g.,hyaluronic acid, dermatan, chondroitin, keratan, heparan); and finally proteoglycans, which have been closely associated with fundamental cellular processes, cell attachment and growth, and cell receptor signaling/binding (e.g.,chondroitin sulfate, heparin sulfate).[20,21]

1.4 Schwann cells

Glial cells are the main neuronal support cells of the nervous system with the SCs (e.g., S42 cell line, or primary SC isolated from the sciatic nerve) being the most widely studied for PNS regeneration.[22–27] These cells contribute to neuron pathfinding by guiding their axons between the proximal to distal stumps, and by producing myelin sheath to protect them. SCs are so important to nerve regeneration that further alternatives for them have been explored by using differentiated stem cells (ADSC or iPSC) to SC-like cells[28–31] or BMSC to effect nerve regeneration, either by direct and/or indirect paracrine signaling to express glial markers.[32,33] SCs can be induced from ADSCs cells by addition of glial growth factor and co-culture with SCs.

A key factor when working with cell differentiation and proliferation is cell density, since it has been reported that higher cell density equals an increase of cell-cell interactions, which is also related to the influence of glial growth factor.[34]

Schwann cells (SCs) develop along the following path: Neural crest cells ➔ Precursors of Schwann cells ➔ Immature Schwann cells. Once the immature cells are formed, they give way to two types of Schwann cells: myelinating and non-myelinating.[35] However, despite being two different kinds of cells, once PNI occurs, both types become a phenotype known as "Repair Schwann cells" which send signals to neurons to promote their survival, express components of the ECM (several growth factors) and activate the immune response.[36–38] Given the importance of this type of cell, a large part of the research for the nervous tissue regeneration revolves around finding strategies to improve the adhesion and proliferation of SCs.

1.5 Peripheral Nerve Injury

Peripheral nerve injury (PNI) is defined as damage partial or total to the peripheral nerve tissue that causes the malfunction of the nerve.[39] The main causes for PNIs are the physical trauma, genetic factors, or immune diseases.[40] There are two fundamental categories for the classification of PNIs: the *Seddon classification* that describes pathological damage in a broad way, and the *Sunderlan classification* that groups 5 levels of anatomical damage (See **Figure 1-2**).[39,41] Although peripheral neurons can regenerate, in the case of PNI this depends on the severity and damage of the injury. Specifically, Neurotmesis or Category V involves the complete rupture of the nerve and therefore self-regeneration is not possible. For these cases a surgical intervention is necessary, and the gold standard is the use of autografts. Due to the negative implications that these procedures have, such as the risks of infections, loss of mobility, or additional surgeries; another option is the use of Nerve Guide Conduits (NGCs).[39,41]

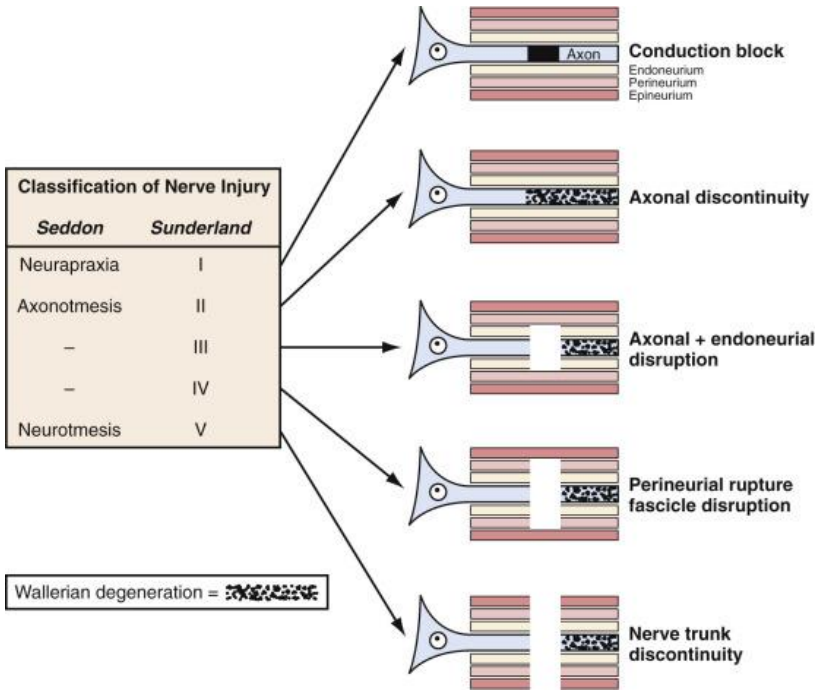

Figure 1-2. The Seddon classification and the 5-levels Sunderland classification of PNIs. [39]

1.6 Nerve Guide Conduits

An Nerve Guide Conduit (NGC) is a cylindrical implant made of synthetic or natural materials that is placed in the lesion to promote tissue regeneration by functioning as a bridge that connects both ends of the gap.[41–43] However, there is a need to improve their performance since they are limited to short lesions (1 to 2 cm) due to the lack of components that autografts can provide.[41] There are three types of NGCs based on the material of manufacture. The NGCs can be of the natural type, made with Collagen, silk or Chitosan for example, synthetics (with PCL or PLLA), or composite that use a combination of polymers either natural-natural, synthetic-synthetic, or natural-synthetic.[42–44]

Collagen is a common protein found in various tissues such as skin and bone.[45] Collagen-based NGCs are ideal for supporting tissue growth or regeneration since they generate a very low

immune response, are easily broken down and absorbed by the body, and can be used as an effective system for drug and protein delivery. For our experimentation processes, these studies will be carried out using a commercial collagen NGC approved by the FDA, generously donated by Integra LifeScience Corporation, whose trade name is NeuraGen® (See **Figure 1-3**).

Figure 1-3. NeuraGen®, a commercial collagen-based NGC.

1.7 The Layer-by-layer method

Layer-by-layer (LbL) is a technique used to produce thin layers or coatings on surfaces, taking advantage of the sequence-specific electrostatic interactions between polyelectrolytes [1][2]. It has been widely used for: biomedical applications [3], corrosion control [3], catalysis [4], drug delivery [5], electrochemical sensing [6], protein purification [7], electrochromism [8], ultrastrong materials [9], optics and optoelectronics [10], among others [11][12][13]. **Figure 1-4** describes the principle of this method.[38,46] These types of polymeric multilayers can be performed on different types of substrates such as silicon, glass, or polystyrene of the cell culture plates.[47]

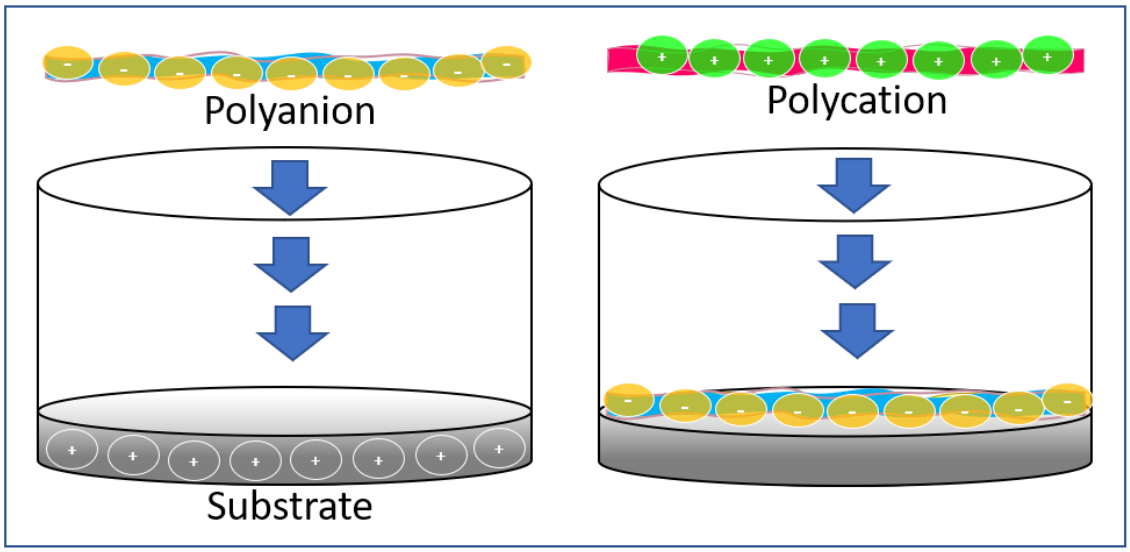

Figure 1-4. Principle of the Layer-by-layer method. The layer deposition occurs due the ionic interactions between polymers with different charges.

LbL coatings can be applied on 3D scaffolds and thus mimic or add to the properties of the ECM. The inclusion of components present in the ECM makes it possible to improve cell proliferation and adhesion.[48,49] Likewise, the coatings will effectively serve as reservoirs and release systems for growth factors, peptides, or drugs.[38]

Previously, we have developed coatings with the HEP/COL combination on polystyrene for cell culture.[50,51] COL, which will be used as a polycation, is characterized as one of the most important components of the ECM. The main function of COL is to provide support to the ECM, therefore, when used as a coating, its immune response will be low, and it will be highly biocompatible.[45] On the other hand, HEP, which has a negative charge and is also one of the components present in the ECM, has been shown to improve axon growth during the regeneration of peripheral nerve, and it has a high affinity with different growth factors.[52]

1.7.1 HEP/COL Multilayers Chemistry and Growth

For natural multilayers of HEP/COL, it was also possible to characterize the physical, chemical, and mechanical properties using Infrared Variable Angle Spectroscopic Ellipsometry (IRVASE) and Atomic Force Microscope (AFM). Our results over the analysis of the chemistry of the multilayers revealed the presence of the characteristic bands of both polymers. **Figure 1-5A** shows the spectrum of 3, 6, 9, and 12 bilayers. The intensity of the peaks is more defined as the number of bilayers increases. For 12 bilayers of HEP/COL the spectrum is more defined, observing the characteristic peaks of both polymers. For both collagen and heparin, the amide I or NH_2 peak 1628 cm^{-1}, and the amide II peak at 1512 cm^{-1} are observed [15][50][51][52]. In this spectrum, it is also possible to identify other characteristic peaks of HEP such as: CH_2 scissoring at 1442 cm^{-1}, SO_3^- at 1211 cm^{-1}, C-N stretching at 1072 cm^{-1} & 1026 cm^{-1}, and the C-O-S stretching vibration at approximately 987 cm^{-1} [15][49]. Thus, the characteristic peaks of collagen and heparin are observed. Similar results are presented by N. Huang and his team when they prepared multilayers of collagen type I and unfractioned heparin over titanium substrates [35][34]. In these studies, they used HEP/COL films as an anticoagulant coating over titanium cardiovascular implants [34]. They also investigated the effect on coagulation of the degradation of the HEP/COL coating [35]. Of note, we were not able to obtain spectra of any of the multilayered films using the FTIR-ATR equipment.

For HEP/COL films, the behavior of growth and roughness shows a linear tendency with increasing number of layers (**Figure 1-5B and 1-5C**). Thicknesses of 44.72 nm, 91.26 nm, 128.8 nm, and 162.44 nm were obtained for 3, 6, 9 and 12 bilayers, respectively (**Figure 1-5B**). An average of 12.66 nm in increase of thickness per bilayer was observed. A significant difference of $p < 0.01$ in the thickness measurements between 6, 9, and 12 multilayers compared with 3 bilayers is observed. Also, a significant difference of $p < 0.05$ was obtained between 9 and 12

bilayers. Jian Ji and her team, who also worked with a HEP/COL system [39], found the same linear behavior in the construction of the films. In their work, they used low molecular weight heparin and collagen type I from bovine cartilage. They dissolved the polymers in acetate buffer solution (0.018 M NaAc, 0.082 M HAc, 0.14 M NaCl, pH 4.0) at 1 mg/mL. Their ellipsometric results showed a thickness of approximately 14 nm for one bilayer, which is close to our results.

Analyzing the roughness and the topographic images (**Figure 1-5C** and **1-5D**), it is possible to observe that as the number of bilayers increases the roughness also increases. For 3, 6, and 9 bilayers of HEP/COL, our results show roughness of 33.58 nm, 101.66 nm, and 163.06 nm, respectively. A significant difference of $p < 0.01$ in the roughness measurements between 6, 9 and 12 multilayers compared with 3 bilayers is observed. A significant difference of $p < 0.05$ was obtained between 6, 9, and 12 bilayers (**Figure 1-5C**). Chau-Chang Chou and his group [36] in one of their works evaluated 5 and 15 bilayers of HEP/COL to study the blood compatibility and adhesion of multilayers coated on cp-Ti substrates. They used heparin sodium salt at 5 mg/mL in DI water and collagen type I derived from bovine Achilles tendon dissolved in 0.2 M acetic acid at 2.5 mg/mL in DI water at pH 4. Their results obtained for roughness by AFM indicated an average of 110 nm for the multilayer system composed of 5 bilayers, which resembles a close relationship to 101.66 nm obtained for our polymeric system of 6 bilayers.

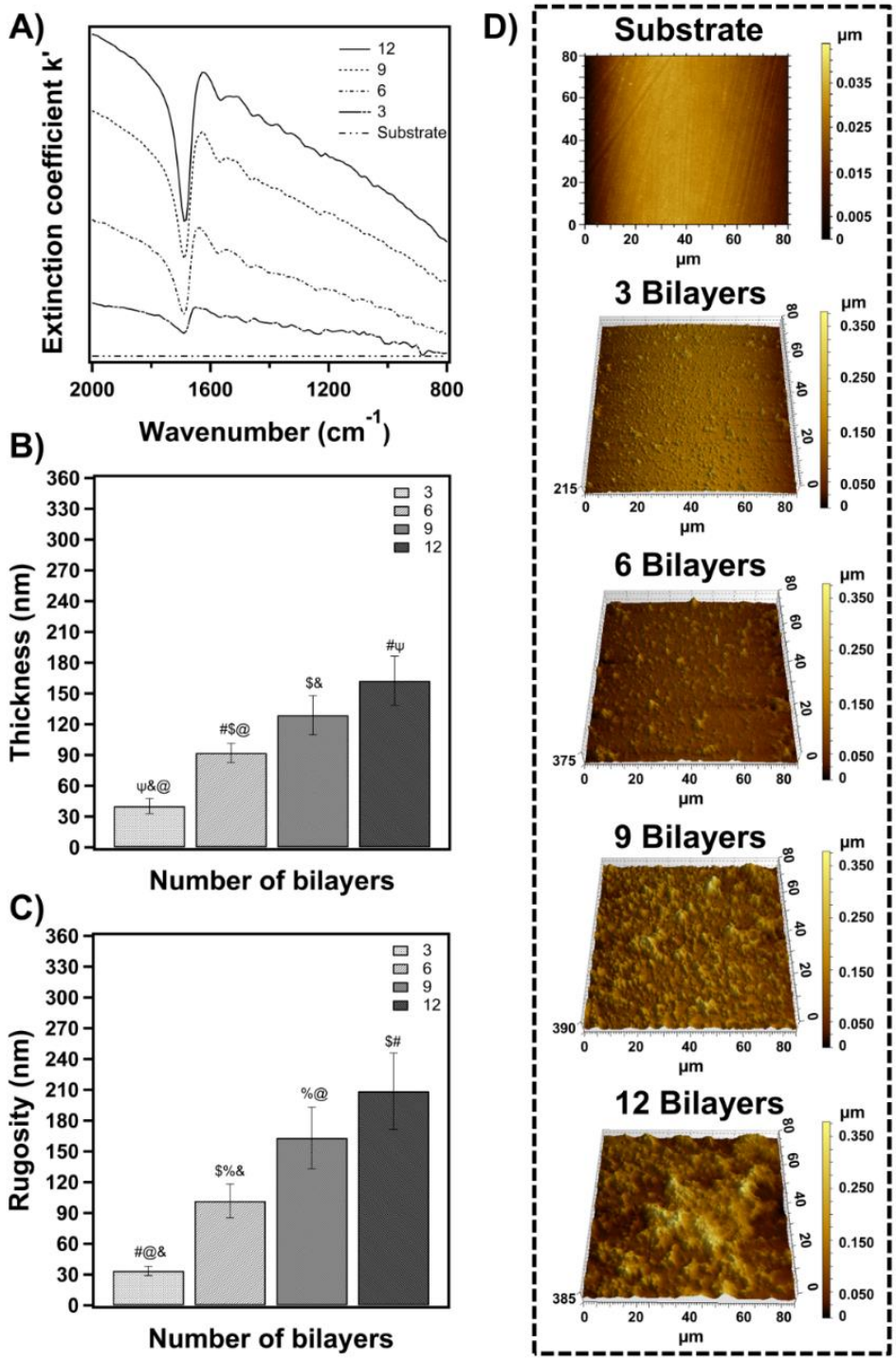

Figure 1-5. Multilayer growth, chemical, and physical characteristics for HEP/COL system by IRVASE. A) Spectrum of plain substrate, 3, 6, 9, and 12 bilayers, B) Thickness vs. number of bilayers, C) Roughness vs. number of bilayers and D) Surface morphology as measured by AFM of: Substrate, 3 bilayers, 6 bilayers, 9 bilayers and 12 bilayers. The error bars indicate the standard deviation of the samples as is described in the materials and methods section. The p-values < 0.01 are represented by #, @, &, ψ and Θ. The p-values < 0.05 are represented by $, % and !. The bars that have the same symbol are statistically different. Reprinted from[51], Copyright 2018, with permission from Elsevier.

1.8 References

[1] J.W. Griffin, M.C. v. Hogan, A.B. Chhabra, D.N. Deal, Peripheral nerve repair and reconstruction, Journal of Bone and Joint Surgery. 95 (2013) 2144–2151. https://doi.org/10.2106/JBJS.L.00704.

[2] H.E. Resnick, K.B. Stansberry, T.B. Harris, M. Tirivedi, K. Smith, P. Morgan, A.I. Vinik, Diabetes, peripheral neuropathy, and old age disability, Muscle Nerve. 25 (2002) 43–50. https://doi.org/10.1002/mus.1217.

[3] D. Grinsell, C.P. Keating, Peripheral Nerve Reconstruction after Injury: A Review of Clinical and Experimental Therapies, Biomed Res Int. 2014 (2014). https://doi.org/10.1155/2014/698256.

[4] Peripheral Neuropathy Fact Sheet, (n.d.).

[5] C.A. Taylor, D. Braza, J.B. Rice, T. Dillingham, The incidence of peripheral nerve injury in extremity trauma, Am J Phys Med Rehabil. 87 (2008) 381–385. https://doi.org/10.1097/PHM.0b013e31815e6370.

[6] S.H. Choi, Y.H. Kim, M. Hebisch, C. Sliwinski, S. Lee, C. D'Avanzo, H. Chen, B. Hooli, C. Asselin, J. Muffat, J.B. Klee, C. Zhang, B.J. Wainger, M. Peitz, D.M. Kovacs, C.J. Woolf, S.L. Wagner, R.E. Tanzi, D.Y. Kim, A three-dimensional human neural cell culture model of Alzheimer's disease, Nature. 515 (2014) 274–278. https://doi.org/10.1038/nature13800.

[7] T. Alberio, L. Lopiano, M. Fasano, Cellular models to investigate biochemical pathways in Parkinson's disease, FEBS Journal. 279 (2012) 1146–1155. https://doi.org/10.1111/j.1742-4658.2012.08516.x.

[8] M. Ravi, V. Paramesh, S.R. Kaviya, E. Anuradha, F.D. Paul Solomon, 3D cell culture systems: Advantages and applications, J Cell Physiol. 230 (2015) 16–26. https://doi.org/10.1002/jcp.24683.

[9] 2014 ASCB/IFCB Meeting abstracts, Mol Biol Cell. 25 (2014) 3987–3987. https://doi.org/10.1091/mbc.e14-10-1437.

[10] G. Kemmperman, F.H. Gages, New nerve cells for the adult brain, Sci Am. 280 (1998) 48–53.

[11] B.D. Simons, H. Clevers, Strategies for homeostatic stem cell self-renewal in adult tissues, Cell. 145 (2011) 851–862. https://doi.org/10.1016/j.cell.2011.05.033.

[12] L. Tian, M.P. Prabhakaran, S. Ramakrishna, Strategies for regeneration of components of nervous system: scaffolds, cells and biomolecules, Regen Biomater. 2 (2015) 31–45. https://doi.org/10.1093/rb/rbu017.

[13] S. Geuna, S. Raimondo, F. Fregnan, K. Haastert-Talini, C. Grothe, In vitro models for peripheral nerve regeneration, European Journal of Neuroscience. 43 (2016) 287–296. https://doi.org/10.1111/ejn.13054.

[14] R. Kiernan, John, Rajakumar, Barr's the Human Nervous System: an Anatomical Viewpoint, Lippincott, Williams and Wilkins, 2009.

[15] M. Griffin, M. Malahias, S. Hindocha, K.S. Wasim, Peripheral nerve injury: principles for repair and regeneration., Open Orthop J. 8 (2014) 199–203. https://doi.org/10.2174/1874325001408010199.

[16] E.A. Huebner, S.M. Strittmatter, Axon Regeneration in the Peripheral and Central Nervous Systems, in: E. Koenig (Ed.), Cell Biology of the Axon, Springer Berlin Heidelberg, Berlin, Heidelberg, 2009: pp. 305–360. https://doi.org/10.1007/400_2009_19.

[17] J.W. GRIFFIN, R. GEORGE, T. HO, Macrophage Systems in Peripheral Nerves. A Review, J Neuropathol Exp Neurol. 52 (1993) 553–560. https://doi.org/10.1097/00005072-199311000-00001.

[18] M.G. Burnett, E.L. Zager, M.A.R.K.G.B. Urnett, E.R.I.C.L.Z. Ager, Pathophysiology of peripheral nerve injury: a brief review, Neurosurg Focus. 16 (2004) 1–7. https://doi.org/10.3171/foc.2004.16.5.2.

[19] R.J.S. R. Shane Tubbs, Elias Rizk, Mohammadali M. Shoja, Marios Loukas, Nicholas Barbaro, Nerves and Nerve Injuries: Vol 2: Pain, Treatment, Injury, Disease and Future Directions, Academic Press, 2015.

[20] R. Rutka, James, Rosenblum, Mark, APODACA, GERARD, stern, The extracellular matrix of the central and peripheral nervous systems: structure and function, 69 (1988) 155–170.

[21] S. Carbonetto, The extracellular matrix of the nervous system, Trends Neurosci. 7 (1984) 382–387. https://doi.org/10.1016/S0166-2236(84)80061-2.

[22] G. Li, L. Zhang, C. Wang, X. Zhao, C. Zhu, Y. Zheng, Y. Wang, Y. Zhao, Y. Yang, Effect of silanization on chitosan porous scaffolds for peripheral nerve regeneration, Carbohydr Polym. 101 (2014) 718–726. https://doi.org/10.1016/j.carbpol.2013.09.064.

[23] C.J. Pateman, A.J. Harding, A. Glen, C.S. Taylor, C.R. Christmas, P.P. Robinson, S. Rimmer, F.M. Boissonade, F. Claeyssens, J.W. Haycock, Nerve guides manufactured from photocurable polymers to aid peripheral nerve repair, Biomaterials. 49 (2015) 77–89. https://doi.org/10.1016/j.biomaterials.2015.01.055.

[24] M.F.B. Daud, K.C. Pawar, F. Claeyssens, A.J. Ryan, J.W. Haycock, An aligned 3D neuronal-glial co-culture model for peripheral nerve studies, Biomaterials. 33 (2012) 5901–5913. https://doi.org/10.1016/j.biomaterials.2012.05.008.

[25] J.I. Kim, T.I. Hwang, L.E. Aguilar, C.H. Park, C.S. Kim, A Controlled Design of Aligned and Random Nanofibers for 3D Bi-functionalized Nerve Conduits Fabricated via a Novel Electrospinning Set-up, Sci Rep. 6 (2016) 23761. https://doi.org/10.1038/srep23761.

[26] M. Georgiou, S.C.J. Bunting, H.A. Davies, A.J. Loughlin, J.P. Golding, J.B. Phillips, Engineered neural tissue for peripheral nerve repair, Biomaterials. 34 (2013) 7335–7343. https://doi.org/10.1016/j.biomaterials.2013.06.025.

[27] B.N. Johnson, K.Z. Lancaster, G. Zhen, J. He, M.K. Gupta, Y.L. Kong, E.A. Engel, K.D. Krick, A. Ju, F. Meng, L.W. Enquist, X. Jia, M.C. McAlpine, 3D Printed Anatomical Nerve Regeneration Pathways, Adv Funct Mater. 25 (2015) 6205–6217. https://doi.org/10.1002/adfm.201501760.

[28] C.M.A.P. Schuh, T.J. Morton, A. Banerjee, C. Grasl, H. Schima, R. Schmidhammer, H. Redl, D. Ruenzler, Activated Schwann Cell-Like Cells on Aligned Fibrin-Poly(Lactic-Co-Glycolic Acid) Structures: A Novel Construct for Application in Peripheral Nerve Regeneration, Cells Tissues Organs. 200 (2015) 287–299. https://doi.org/10.1159/000437091.

[29] A. Wang, Z. Tang, I.-H. Park, Y. Zhu, S. Patel, G.Q. Daley, S. Li, Induced pluripotent stem cells for neural tissue engineering, Biomaterials. 32 (2011) 5023–5032. https://doi.org/10.1016/j.biomaterials.2011.03.070.

[30] A. Mobasseri, A. Faroni, B.M. Minogue, S. Downes, G. Terenghi, A.J. Reid, Polymer scaffolds with preferential parallel grooves enhance nerve regeneration., Tissue Eng Part A. 21 (2015) 1152–62. https://doi.org/10.1089/ten.TEA.2014.0266.

[31] Y. Xu, Z. Zhang, X. Chen, R. Li, D. Li, S. Feng, A silk fibroin/collagen nerve scaffold seeded with a co-culture of schwann cells and adipose-derived stem cells for sciatic nerve regeneration, PLoS One. 11 (2016) 1–11. https://doi.org/10.1371/journal.pone.0147184.

[32] J.T. Oliveira, K. Mostacada, S. de Lima, A.M.B. Martinez, Bone marrow mesenchymal stem cell transplantation for improving nerve regeneration, 1st ed., Elsevier Inc., 2013. https://doi.org/10.1016/B978-0-12-410499-0.00003-4.

[33] M. Tohill, C. Mantovani, M. Wiberg, G. Terenghi, Rat bone marrow mesenchymal stem cells express glial markers and stimulate nerve regeneration, Neurosci Lett. 362 (2004) 200–203. https://doi.org/10.1016/j.neulet.2004.03.077.

[34] M.M. Najafabadi, V. Bayati, M. Orazizadeh, M. Hashemitabar, F. Absalan, Impact of cell density on differentiation efficiency of rat adipose-derived stem cells into schwann-like cells, Int J Stem Cells. 9 (2016) 213–220. https://doi.org/10.15283/ijsc16031.

[35] R. Mirsky, K.R. Jessen, Schwann cell development, differentiation and myelination, Curr Opin Neurobiol. 6 (1996) 89–96. https://doi.org/10.1016/S0959-4388(96)80013-4.

[36] C. Cheng, D.W. Zochodne, In vivo proliferation, migration and phenotypic changes of Schwann cells in the presence of myelinated fibers, Neuroscience. 115 (2002) 321–329. https://doi.org/10.1016/s0306-4522(02)00291-9.

[37] K.R. Jessen, R. Mirsky, The repair Schwann cell and its function in regenerating, J Physiol. 594 (2016) 3521–3531. https://doi.org/10.1113/JP270874.

[38] L. Pinzon-Herrera, J. Mendez-Vega, A. Mulero-Russe, D.A. Castilla-Casadiego, J. Almodovar, Real-time monitoring of human Schwann cells on heparin-collagen coatings reveals enhanced adhesion and growth factor response, J Mater Chem B. 8 (2020) 8809–8819. https://doi.org/10.1039/d0tb01454k.

[39] S.J. Bunn, CHARACTERIZATION OF SCHWANN CELLS STIMULATED BY DC ELECTRIC FIELDS, 2019.

[40] H. Jiang, Y. Qian, C. Fan, Y. Ouyang, Polymeric Guide Conduits for Peripheral Nerve Tissue Engineering, Front Bioeng Biotechnol. 8 (2020) 1–8. https://doi.org/10.3389/fbioe.2020.582646.

[41] B. Pfister, T. Gordon, J.R. Loverde, A.S. Kochar, S.E. Mackinnon, D.K. Cullen, Biomedical Engineering Strategies for Peripheral Nerve Repair: Surgical Applications, State of the Art, and Future Challenges, Crit Rev Biomed Eng. 39 (2011) 81–124. https://doi.org/10.1615/CritRevBiomedEng.v39.i2.20.

[42] H. Jiang, Y. Qian, C. Fan, Y. Ouyang, Polymeric Guide Conduits for Peripheral Nerve Tissue Engineering, Front Bioeng Biotechnol. 8 (2020). https://doi.org/10.3389/fbioe.2020.582646.

[43] N.U. Kang, S.J. Lee, S.J. Gwak, Fabrication Techniques of Nerve Guidance Conduits for Nerve Regeneration, Yonsei Med J. 63 (2022) 114–123. https://doi.org/10.3349/ymj.2022.63.2.114.

[44] A. Magaz, A. Faroni, J.E. Gough, A.J. Reid, X. Li, J.J. Blaker, Bioactive Silk-Based Nerve Guidance Conduits for Augmenting Peripheral Nerve Repair, Adv Healthc Mater. 7 (2018). https://doi.org/10.1002/adhm.201800308.

[45] R. Ayala-caminero, L. Pinzón-herrera, C.A. Rivera Martinez, J. Almodovar, Polymeric scaffolds for three-dimensional culture of nerve cells: a model of peripheral nerve regeneration, MRS Commun. 7 (2017) 391–415. https://doi.org/10.1557/mrc.2017.90.

[46] Z. Tang, Y. Wang, P. Podsiadlo, N.A. Kotov, Biomedical Applications of Layer-by-Layer Assembly: From Biomimetics to Tissue Engineering, Advanced Materials. 18 (2006) 3203–3224. https://doi.org/10.1002/adma.200600113.

[47] J.L. Lutkenhaus, P.T. Hammond, Electrochemically enabled polyelectrolyte multilayer devices: From fuel cells to sensors, Soft Matter. 3 (2007) 804–816. https://doi.org/10.1039/b701203a.

[48] P. Gentile, I. Carmagnola, T. Nardo, V. Chiono, Layer-by-layer assembly for biomedical applications in the last decade, Nanotechnology. 26 (2015) 1–21. https://doi.org/10.1088/0957-4484/26/42/422001.

[49] J. Almodóvar, L.W. Place, J. Gogolski, K. Erickson, M.J. Kipper, Layer-by-layer assembly of polysaccharide-based polyelectrolyte multilayers: a spectroscopic study of hydrophilicity, composition, and ion pairing, Biomacromolecules. 12 (2011) 2755–2765. https://doi.org/10.1021/bm200519y.

[50] D. Castilla-Casadiego, J. Garcia, A.J. Garcia, J. Almodóvar, Heparin/Collagen Coatings Improve Human Mesenchymal Stromal Cell Response to Interferon Gamma, ACS Biomater Sci Eng. 5 (2019) 2793–2803.

[51] D.A. Castilla-Casadiego, L. Pinzon-Herrera, M. Perez-Perez, B.A. Quiñones-Colón, D. Suleiman, J. Almodovar, Simultaneous characterization of physical, chemical, and thermal properties of polymeric multilayers using infrared spectroscopic ellipsometry, Colloids and Surfaces A. 553 (2018) 155–168. https://doi.org/10.1016/j.colsurfa.2018.05.052.

[52] K. Zhang, D. Huang, Z. Yan, C. Wang, Heparin/collagen encapsulating nerve growth factor multilayers coated aligned PLLA nanofibrous scaffolds for nerve tissue engineering, J Biomed Mater Res A. 105A (2017) 1900–1910. https://doi.org/10.1002/jbm.a.36053.

CHAPTER 2. Real-time monitoring of human Schwann cells on heparin-collagen coatings reveals enhanced adhesion and growth factor response

2.1 Abstract

In this work, we evaluate the enhancing effect of six bilayers of heparin/collagen $(HEP/COL)_6$ layer-by-layer coatings on human Schwann cell (hSCs) adhesion and proliferation in the presence or absence of nerve growth factor (NGF). hSCs behavior and in vitro bioactivity were studied during six days of culture using end-point viability and proliferation assays as well as an impedance-based real-time monitoring system. An end-point viability assay revealed that hSCs cultured on the $(HEP/COL)_6$ coatings increased their growth by more than 230% compared to controls. However, an EdU proliferation assay revealed that the proliferation rate of hSCs in all conditions were similar, with 45% of cells proliferating after 18 hours of incubation. Fluorescence microscopy revealed that hSCs spreading was similar between the tissue culture plastic control and the $(HEP/COL)_6$. The presence of NGF in solution resulted in cells with a larger spread area. Real-time monitoring of hSCs seeded on $(HEP/COL)_6$ with and without NGF reveals that initial cell adhesion is improved by the presence of the $(HEP/COL)_6$ coatings, and it is further improved by the presence of NGF. Our results suggest that $(HEP/COL)_6$ coatings enhance Schwann cell behavior and response to NGF. This simple modification could be applied to current nerve regeneration strategies to improve the repair of damaged nerve.

2.2 Introduction

Peripheral nerve injuries exceed $150 billion annually in medical expenses in the US, and surgeries with the use of autografts (a nerve from the same patient) are the "gold standard" to treat these types of injuries. However, the use of grafts can cause pain, scarring, or other diseases

at the donor site.[1–3] One of the biggest challenges is to replace the autograft with an artificial guide conduit, which can repair significant gaps (lesions larger than 1 cm). This achievement would only be possible if the conduit surface enhances the development and interactions of cells with the extracellular matrix (ECM).[4,5]

When an injury to the peripheral nervous system (PNS) occurs, a crucial stage of collaboration between macrophages and neurons is facilitated by human Schwann cells (hSCs).[6] Schwann cells arise from a group of neural crest cells, which in turn generate the precursors of Schwann cells. Then, these precursors become another type of cell known as immature Schwann cells. Finally, once formed, immature cells produce two types of Schwann cells: myelinating and non-myelinating.[7] A nerve lesion causes Schwann cells (of both kinds) to become a phenotype responsible for promoting repair, by sending the signals necessary for neuron survival.[8] Additionally, Schwann cells develop other essential functions such as the activation of the immune response,[6] the expression of components of the ECM, and efficient destruction of remains of damaged peripheral nerve.[9] Mature myelin-forming Schwann cells are responsible for regulating the gene expression for the production of myelin. Similarly, Schwann cells release several cytokines and neurotrophic factors such as the nerve growth factor (NGF), brain-derived neurotrophic factor (BDNF), and ciliary neurotrophic factor (CNTF). In this way, Schwann cells contribute greatly to the replacement of injured neurons and allow the extension of the axon.[1,8,10–13] Since Schwann cells functions involve a series of challenging steps, this type of cells are essential for the repair of PNS lesions. Therefore, there is a need to find strategies at the therapeutic level to improve hSCs response and proliferation.[12,14]

The ECM is composed of a series of biomacromolecules such as proteins, glycoproteins, proteoglycans, and polysaccharides.[15] Therefore, surfaces interacting with cells must have properties similar to the ECM.[16] For surface improvement, the layer-by-layer (LbL) technique

has gained significant importance in the last two decades, thanks to the manufacturing of stable and biocompatible coatings.[17–19] LbL method uses electrostatic interactions to build multilayers that modify the surface properties. In this manner, cellular response is favored through the interaction with natural or synthetic polymers.[17] An important application of the LbL technique is the modification of biodegradable 3D scaffolds to mimic native ECM and enhance cell growth and adhesion. Also, the scaffolds serve as a reservoir for the storage and release of growth factors.[19,20] The technique is relatively simple, and the coatings are achieved by a sequential changing of the net surface charge, which allows the adsorption of the polyelectrolytes by the interactions of opposite charges (**Figure 2-1A**).[17,21] Additionally, because of the nature of the polymers used, a wide variety of *in vitro* assays can be made without the stability of the films being affected by culture media.[22,23] Furthermore, not only polymers but also peptides, proteins,[18,24–26] viruses,[27] or drugs[2,28] can be deposited in LbL films, which makes the technique even more versatile.

One of the major components of the ECM is collagen.[29] This natural protein provides the structural basis for the ECM, is biocompatible, and elicits a low immune response.[29] Additionally, collagen allows the manufacturing of different types of scaffolds such as fibers, sponges, or hydrogels, and is currently used efficiently in nerve tissue regeneration.[30,31] On the other hand, heparin is a polysaccharide of great use. This polymer is highly present in the ECM and has a strong negative charge as well as a specific affinity with multiple growth factors. Heparin has also been shown to improve the growth of axons in peripheral nerve lesions.[24] Our group has developed heparin/collagen (HEP/COL) LbL coatings as surfaces for cell culture.[18,21] Specifically, we have shown that mesenchymal stromal cells have an enhanced response to growth factors when cultured on these coatings.[18] In our previous work, we demonstrated that the chemistry of the coatings is maintained for temperatures between 25 to 37°C. Also, as the number of bilayers increases, the growth of bilayers occurs in a linear manner,

which allows the coatings to be adjusted to the desired application.[21] Spectroscopic ellipsometry and quartz crystal microbalance with dissipation have been used to measure the stability of HEP/COL LbL coatings. Li et al. showed that after 18 hours in incubation in phosphate-buffered saline, five bilayers of HEP/COL coatings remained stable.[32] In a recent work, Cifuentes et al. demonstrated that after 30 days of manufacture, the characteristic functional groups for heparin and collagen were present confirming the structural presence of the coatings.[23] HEP/COL LbL coatings are being used[33] with the incorporation of neurotrophic factors such as NGF to release the neuropeptide by diffusion and promote cell regeneration more efficiently.[24]

This research aims to improve the proliferation, adhesion, and viability of hSCs. The action of surfaces modified by LbL coatings minimizes any adverse effect on development and cell morphology. In the same way, this work seeks to study the real-time behavior of cultured cells on heparin-collagen films. We evaluated the response and real-time growth of hSCs over four conditions including tissue culture polystyrene (TCPS) and TCPS coated with six bilayers of HEP/COL combination, which will be noted as $(HEP/COL)_6$ (see **Scheme 2-1**). We also used NGF added to the culture medium as a supplement. Viability, proliferation, morphology, and adhesion were analyzed using specific assays and by fluorescent microscopy. Finally, we evaluated whether the the bioactivity of the NGF was altered by the $(HEP/COL)_6$ coatings by culturing PC-12 cells in the presence or absence of NGF.

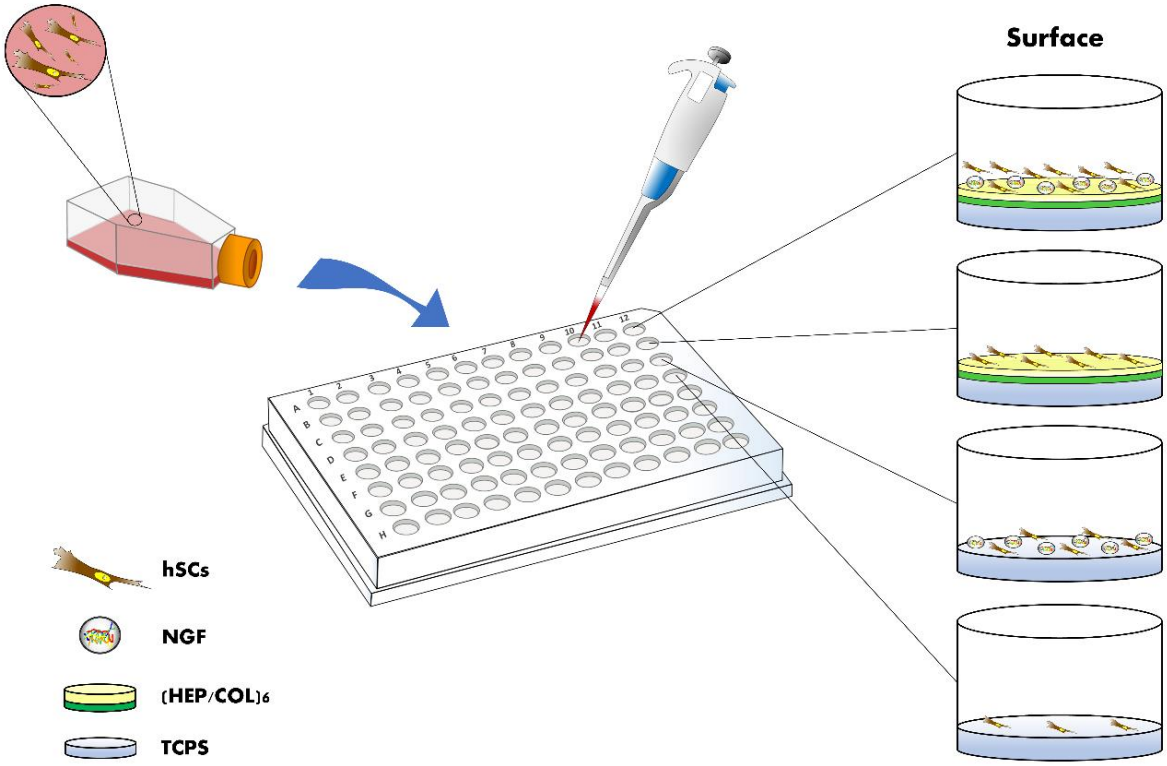

Scheme 2-1. Schematic illustration for experimental study of hSCs cultured on four different surfaces: TCPS, TCPS + NGF in solution, $(HEP/COL)_6$, and $(HEP/COL)_6$ + NGF in solution. Reproduced from [53]with permission from the Royal Society of Chemistry.

2.2 Materials and Methods

2.2.1 Cell culture

Human Schwann cells from ATCC® (sNF96.2 ATCC® CRL-2884™), from a 28-year-old male, were used between passages 17-20. hSCs were grown in Dulbecco's Modified Eagle's Medium from SIGMA-ALDRICH® (Cat. # D5648) containing 10% Fetal bovine serum from Gibco® (Cat. # 10-437-028),1% Penicillin-streptomycin from SIGMA-ALDRICH® (Cat. # P4333) and supplemented with sodium bicarbonate and sodium pyruvate. PC-12 Cells from ATCC (ATCC® CRL-1721™), from a male rat, were used between passages 5-7. PC-12 cells were grown in RPMI-1640 Medium from SIGMA-ALDRICH® (Cat. # R6504) containing 5% Fetal bovine serum

from Gibco® (Cat. # 10-437-028), 1% Penicillin-streptomycin from SIGMA-ALDRICH® (Cat. # P4333) and supplemented with sodium bicarbonate. Both types of cells were incubated in a humid incubator at 37°C with an air atmosphere containing 5% CO_2.

2.2.2 LbL coatings fabrication

$(HEP/COL)_6$ were constructed as described in our previous works.[18,21] Briefly, Lyophilized type I collagen sponges (generously donated by Integra Lifesciences Holdings Corporation, Añasco, PR), sodium heparin produced by Celsius Laboratories, Inc. (Cat. # PH3005) and poly-(ethylene imine) (PEI) (50% solution in water, Mw ≈ 750,000) from Sigma-Aldrich (Cat. # P3143) were used to perform the multilayer polymer coatings in the wells of microplates. All polymer solutions were prepared at a concentration of 1.0 mg/mL in sodium acetate buffer (at pH=5 for HEP and PEI, and pH=4 for COL). We used sodium acetate buffer at pH=5 as the washing solution, and ultra-pure water from a MilliporeSigma™ Direct-Q™ 3 (Cat. # ZRQSVP3US) at 18.2 MΩ-cm to prepare the solutions. To produce a strong positive charge, we performed an anchoring layer prior to HEP/COL coatings fabrication by adding the PEI solution for 15 minutes to each well and following with a washing step for 3 minutes. After this, HEP and COL were deposited for 5 minutes alternating with an intermediate wash of 3 minutes. This procedure was done to form one bilayer and was repeated 6 times to reach $(HEP/COL)_6$. As a final step, a wash was performed with phosphate-buffered saline (PBS 1X) from Thermo Scientific™ (Cat. # 28372) for 3 minutes, and the wells were left with 200 µL of PBS. A UV sterilization step was performed for 10 minutes before cell culture.

2.2.3 Physicochemical characterization of $(HEP/COL)_6$

2.2.3.1 Chemical composition and thickness of $(HEP/COL)_6$

$(HEP/COL)_6$ were created on silicon wafers from WRS Materials (resistivity of 5–10 Ohm-cm and thickness between 356–406 µm). A StratoSequence VI Robotic Unit was used for the automated multilayers processing on silicon according to the method illustrated in Figure 1A. After drying the samples completely, an Infrared Variable Angle Spectroscopic Ellipsometry device (IR-VASE® - Mark II, J.A. Woollam Co., Inc. IR-VASE, Lincoln, Nebraska) was used to determine the chemical composition and thickness of the multilayers. The analysis was performed with a DTGS detector under the following parameters described in one of our previous publications:[21] a wavenumber range from 800 – 1800 cm-1, a spectral resolution of 16 cm-1, an angle of incidence of 70°, 200 scans per cycle, 2 cycles, a bandwidth of 0.01 µm, a minimum intensity ratio of 2, zone average as polarizer, single position as RCE analyzer, and sample type as Isotropic.

2.2.3.2 Topography analysis of $(HEP/COL)_6$

An Agilent Atomic Force Microscope (AFM), model 5500 (Keysight Technologies, Santa Rosa, CA), and a Laser microscope & 3D profile measurement (VHX-7000 Series Digital Microscope) from Keyence were used for the topographical characterization of (HEP/COL)6. To analyze the topography by AFM, measurements were performed using a silicon SPM sensor cantilever for contact mode (Cat. # N9832B). All measurements were carried out in the air, under ambient conditions, and each image measurements on a sample correspond to 512 × 512 pixels. The scanning speed used was 1.96 lines/s. The size of the scanned area was 80 x 80 µm.

2.2.3.3 Surface charge of $(HEP/COL)_6$

The surface charge of 1.5, 3, 4.5, and 6 bilayers was analyzed by Z-potential studies using an instrument from Beckman Coulter Delsa NanoHC, Brea, Ca (Cat. # A53879). A flat surface cell (Beckman Coulter P/N A54117) was employed for the determination of zeta-potential on the polymeric surface. Dry samples were immersed in the feed solution with predefined pH value for the measurement of zeta-potential. NaCl was used for calibration. Triple measurements were carried out.

2.2.3.4 Qualitative colorimetric determination of heparin deposited within $(HEP/COL)_6$

We prepared wells with 1, 2, 3, 4, 5, and 6 bilayers on 24-Well Corning™ Costar™ flat-bottom polystyrene microplates (Fisher Cat. # 07-200-740, area of 1.9 cm^2/well) following the procedure described in Section 2.2 (LbL coatings fabrication). The microplate was dried for 3 hours in a laminar flow hood. Once the samples were completely dry, 1 mL of Taylor's Blue dye solution was added on each well. Taylor's Blue dye solution was prepared by adding 0.76 g of Glycine Ultrapure Bioreagent from J.T. Baker (VWR Cat. # JT4059-0), 0.59 g of Sodium chloride (NaCl) from VWR Chemicals (Cat. # BDH9286-500G), and 4 mg of 1,9-Dimethyl-Methylene Blue zinc chloride double salt (Taylor’s Blue dye) from Sigma-Aldrich (Cat. # 341088-1G) in 23.75 mL of 0.1 M HCl and completed with deionized water up to 250 mL. Reaction between heparin and Taylor's blue dye solution was allowed by incubation at room temperature for 30 minutes. Then, we removed Taylor’s blue dye solution and added to each well 1 mL of the Dissociating agent solution (3M GuHCl solution), which was prepared by dissolving 5.74 g of Guanidinium chloride from TCI (VWR Cat. # TCG0197-025G) in 20 ml of PBS. The microplates were shaken at 750 rpm for 10 minutes to facilitate the release of the heparin molecules adhered to Taylor's Blue dye

into the dissociating solution. 200 µL of each sample was transferred to a 96-well Corning™ Costar™ flat-bottom polystyrene microplate (Fisher Cat. # 07-200-87), and we read the absorbance at 653 nm at the endpoint using a BioTek Multi-Mode Microplate Reader (Model Synergy™ 2).

2.2.4 Experimental design

Time points and the initial number of cells were selected according to the nature and sensitivity of the specific method used and by performing a preliminary qualitative trial for cell confluence after three days of cell culture on an uncovered surface and on $(HEP/COL)_6$ (Figure 2-S1, Appendix).

2.2.4.1 Human Schwann cells culture conditions

$(HEP/COL)_6$ were constructed on Corning™ 3603 96-Well clear bottom black polystyrene microplates (Fisher Cat. # 07-200-565, cell growth area of 0.32 cm^2 per well) to culture hSCs and analyze their behavior under different conditions. In this study, we analyzed cell proliferation, viability, and morphology in 2 different conditions: on $(HEP/COL)_6$ with and without recombinant human beta nerve growth factor (NGF) from R&D Systems (Cat. # 256-GF/CF) added to the culture medium. Cell cultures were also performed as the controls on TCPS with and without NGF. All the cultures were done in a quadruplicated manner for 3 and 6 days. For cultures with NGF in solution, NGF was evaluated at a concentration of 10 ng/mL dissolved in the culture medium. This concentration was determined by a preliminary study and consulting the literature.[34–36]

2.2.4.2 Human Schwann cells viability on $(HEP/COL)_6$

We quantitatively measured hSCs viability using the PrestoBlue™ cell viability reagent from Invitrogen (Cat. # A13261). PrestoBlue is modified by the reducing environment of the cells and becomes a fluorescent reagent.37 A concentration of 25000 cells/cm2 was seeded for each condition. After 6 days of culture, the medium was removed, and 100 µL of fresh culture medium was added with PrestoBlue Reagent in a 9:1 ratio according to the protocol of the manufacturer. The cells were incubated for 3 hours, and the fluorescence intensity measurement was determined with a BioTek Multi-Mode Microplate Reader (Model Synergy™ 2). According to the protocol, the reading was made by fluorescence with excitation/emission of 560/590 nm.

2.2.4.3 Human Schwann cells proliferation on $(HEP/COL)_6$

We measured the ability of cells to proliferate using the Click-iT™ Plus EdU Alexa Fluor™ 488 imaging kit from Invitrogen (Cat. # C10637). A concentration of 6250 cells/cm2 was seeded for each of the conditions previously described (see section 2.4.1). After three days of culture, the medium was removed, and EdU solution was added according to the protocol provided by the manufacturer. The EdU solution was left in incubation for 18 hours, and then the samples were washed with PBS and fixed with 3.7% formaldehyde for 15 minutes. The protocol states a permeabilization stage with a 0.5% Triton® X-100 solution and several washes with 3% BSA (bovine serum albumin). Then the Click-iT™ reaction cocktail was added for detecting EdU and followed again by several washes with 3% BSA. An additional stage was performed for nucleus staining with Hoechst 33342 from Invitrogen (Ref. # H3570) and finished with several washes using PBS. A Leica inverted fluorescence microscope (Model: DMIL LED Fluo with a Leica DMFC3000 G camera) was used to take photographs of the cells. A filter with excitation/emission

of 495/519 nm was used to detect Alexa Fluor™ 488. ImageJ software was used to determine, by counting in the images, the percentage of positive nuclei for EdU.

2.2.4.4 Real-time monitoring of human Schwann cells behavior

$(HEP/COL)_6$ were constructed on the wells of an ACEATM E-Plate L8 (Cat. # 300600840, cell growth area of 0.64 cm^2 per well), and hSCs at a concentration of 25000 cells/cm^2 were seeded. hSCs growth was evaluated under three different conditions using LbL coatings: on uncovered sensors, on $(HEP/COL)_6$ and $(HEP/COL)_6$ with NGF. NGF was also evaluated by adding 10 ng/mL to the culture medium. We monitored a cell culture as a control on the surface of uncoated sensors. All assays were done in duplicate. A Real-Time Cell Analyzer (RTCA) iCELLigence instrument from ACEA Biosciences Inc. (Cat. # 380601000) was used to measure real-time cell behavior. According to the iCELLigence Guide protocol described by the manufacturer, the instrument was initially equilibrated in the incubator for 2 hours. There was no condensation formed on the station after that period. The RTCA was used for monitoring cell proliferation and attachment every 10 minutes. The experiment was carried out for 5 days of cell culture (120 hours). We performed fluorescence imaging to analyze cell morphology.

2.2.4.5 Fluorescent imaging for cell morphology and extension

Fluorescent staining to study cell morphology was performed for the detection of the blue fluorescent dye Hoechst 33342 from Invitrogen (Ref. # H3570). This dye stains the nucleic acid because is permeable to the cell. Additionally, we detected the red-orange fluorescent dye ActinRed™ 555 ReadyProbes™ from Invitrogen (Ref. # 37112), which is selective to Actin F (a fundamental component of the cellular cytoskeleton). After three days of culture, the medium was removed, and the cells were fixed with 3.7% formaldehyde solution for 15 minutes. The samples

were washed several times with PBS to continue with a permeabilization stage for 10 minutes with Triton X100. This step allows the entry of the dyes by incubating the cells. ActinRed™ 555 was first added with an incubation period for 30 minutes and then Hoechst 33342 for 10 minutes. Both dyes had washing steps with PBS before and after being added. For cell imaging, we used a Leica inverted fluorescence microscope with a standard DAPI filter (excitation/emission of 350/461 nm) for Hoechst 33342, and a standard TRITC filter (excitation/emission of 540/565 nm) for ActinRed™ 555. Measurement of the cell area in the different cell culture conditions was made using ImageJ software for images at 20X. We took 6 photos for each culture condition. For each photo, 20 cells were randomly selected to obtain a total of 120 measurements per condition.

2.2.5 PC-12 cells qualitative response to $(HEP/COL)_6$

Due to their ability to respond to NGF,[33] PC-12 cells were used in a qualitative test to evaluate the bioactivity of NGF in the presence of $(HEP/COL)_6$. TCPS coated with poly(l-lysine) was used as a control as a known surface to promote adhesion of PC-12 cells. The cultures were carried out with and without NGF. A cell concentration of 25000 cells/cm^2 was used in 96-well plates. The cells were cultured for six days.

2.2.6 Statistical analysis

The results were compared for the conditions where (HEP/COL)6 was used by a one-way analysis of variance (ANOVA). P-values <0.05 were considered statistically significant. The statistical analysis was carried out using SigmaPlot 14 software. The results are presented with the standard error of the mean (SEM).

2.3 Results and Discussion

2.3.1 Characterization of $(HEP/COL)_6$ Layer-by-Layer films

To confirm the chemical deposition of the polymers, $(HEP/COL)_6$ were constructed on flat silicon samples applying the method described in **Figure 2-1A.** The samples were analyzed using an IRVASE to determine the chemical composition of the coatings as well as their thickness. **Figure 2-1B** shows the IRVASE spectrum of $(HEP/COL)_6$. The characteristic peaks for amide I and amide II present in both collagen and heparin can be observed in the approximate regions of 1620 and 1530 cm^{-1}, respectively. Also, some usual peaks for HEP were found, such as the band that represents the CH_2 scissoring close to 1430 cm^{-1}, and SO_3^- in1210 cm^{-1} (Ref. [21]). For this sample we obtained a thickness of 91 nm which is consistent with our previous results.[21]

The spectrum in **Figure 2-1B** confirmed the characteristic bands for heparin and collagen, as described in one of our published work, where this system was thoroughly characterized. [21] We demonstrated that the IRVASE technique is useful for determining the chemical composition of coatings on surfaces. [21] IRVASE results were validated by comparing the spectrum of each polymer obtained by the Fourier Transform Infrared Spectroscopy (FTIR) technique.[21]

The intensity of the peaks increased as the number of bilayers was higher. The same behavior was obtained for the thickness in the HEP/COL bilayers. As the number of bilayers increased, the thickness of the coatings increased linearly with an average of 12 nm per bilayer. [21] In the same way, we were able to identify the effect of temperature on HEP/COL films, and we can affirm that in the temperature range of 25 to 37 ° C, the chemistry and thickness of the coatings is not affected. A temperature higher than 37 °C produces a decrease in the thickness and in the intensity of the characteristic peaks in the spectra, which suggests a possible polymer degradation.[21]

Z-potential measurements also confirmed that HEP/COL multilayers were successfully deposited on the substrate. **Figure 2-1C** shows the charge values of 1.5, 3, 4.5, and 6 bilayers. These results showed that the Z-potentials of the HEP/COL multilayers alternated from negative to positive depending on the layer added. As heparin is a polyanion, this polymer has a negative charge, which can be observed for 1.5 and 4.5 HEP/COL bilayers (See **Figure 2-1C**). Similarly, the formation of the polymeric layers on the surface also was confirmed using the AFM technique and a laser microscope 3D. **Figure 2-1D** shows an AFM image of $(HEP/COL)_6$ after heating the multilayers on the substrate at 37 °C for 30 minutes (simulating temperature of incubation). This image demonstrates that the surface is still coated for the (HEP/COL) films after it is heated at incubation conditions. A 3D image of $(HEP/COL)_6$ maintained at room temperature is shown in **Figure 2-1E**. Like AFM results, the 3D image also reveals the characteristic roughness topography of HEP/COL bilayers, as reported in our recent study,[21] and shows that the coatings occur on most of the surface.

Qualitative determination of heparin contained in (HEP/COL) bilayers was performed using a variation of the Taylor's Blue colorimetric method defined by Ferreira et al.[37] **Figure 2-2** shows the absorbance values obtained for samples with 1 to 6 bilayers constructed in microwells. It was possible to observe the color change in the Taylor's Blue dye solution corresponding to the positive detection of heparin contained in the bottom of the microwells (from blue to purple / violet). A detailed sequence of changes in coloration is explained in the **Figure 2-S2** in the appendix. Finally, the Dissociating agent solution changed from colorless to light blue as the heparin molecules adhered to the dye were dissolved. A higher tone in the range of blue coloration in the Dissociating agent indicates a higher heparin content per bilayer. This behavior could be confirmed by determining the absorbance values of each sample. We found a linear increase in absorbance from 1 to 6 bilayers, 0.17 to 0.39 units, respectively, and it was possible to establish a constant average increase close to 0.043 absorbance units for each bilayer added (**Figure 2-**

2). This result strongly agrees with the behavior of the thickness determined by IR-VASE, which also showed a linear increase related to the number of bilayers.[21]

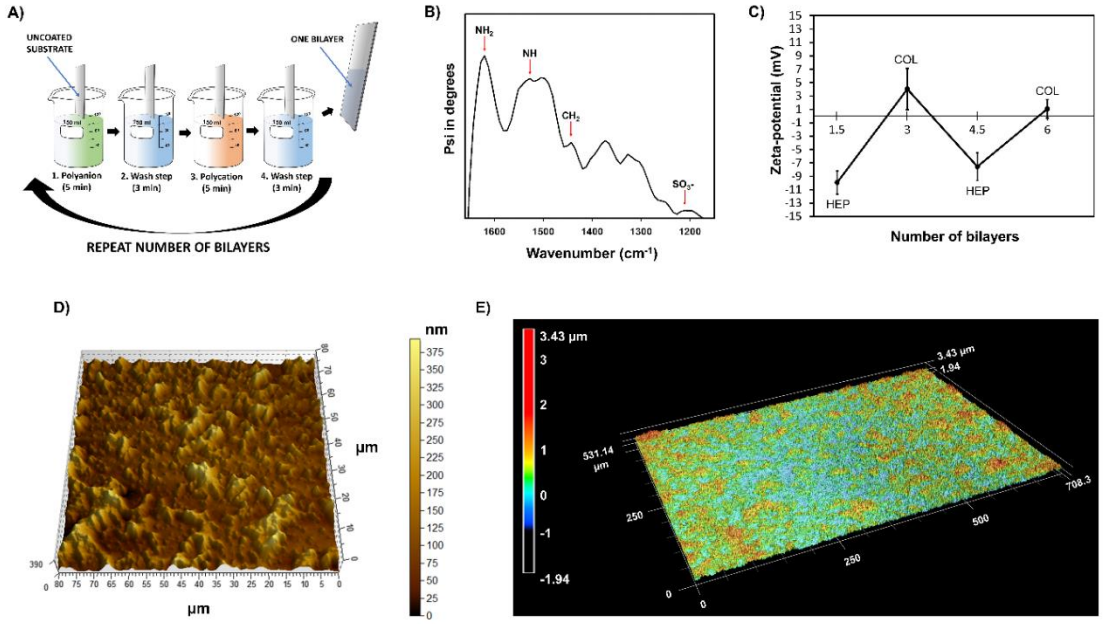

Figure 2-1. A) Scheme of the LBL process by immersion of a flat substrate on beakers. Polyanion and polycation represent the immersion in solution of negatively (heparin) and positively (collagen) charged polymers, respectively, (B) IRVASE spectrum of (HEP/COL)6 on silicon flat substrates, (C) charge values for coatings with 1.5, 3, 4.5, and 6 bilayers of HEP/COL, and (D) AFM image of (HEP/COL)6 at 37 1C, and (E) 3D image of (HEP/COL)6 at 25 1C. Data set for (C) is presented as the mean ± standard deviation of n = 3 samples. Reproduced from [53] with permission from the Royal Society of Chemistry.

2.3.2 PrestoBlue viability assay on $(HEP/COL)_6$ after six days of cell culture

The PrestoBlue reagent was used for indirectly measuring cell viability after six days of culture. A cell concentration of 25000 cells/cm^2 was used in 96-well plates (working volume 200 µm). hSCs were seeded on TCPS and on $(HEP/COL)_6$ with and without NGF.TCPS without NGF was selected as the positive control and its fluorescence intensity was normalized to 100%. We evaluated all other conditions in relation to the positive TCPS control. Cultures on TCPS with NGF showed fluorescence intensity values close to 130%, indicating an approximate increase of 30%

in cell number in the presence of soluble NGF. hSCs viability greatly increases in the culture conditions where $(HEP/COL)_6$ were used. For these two conditions $(HEP/COL)_6$ with and without NGF in solution, the values obtained were 255% and 226%, respectively (**Figure 2-3B**).

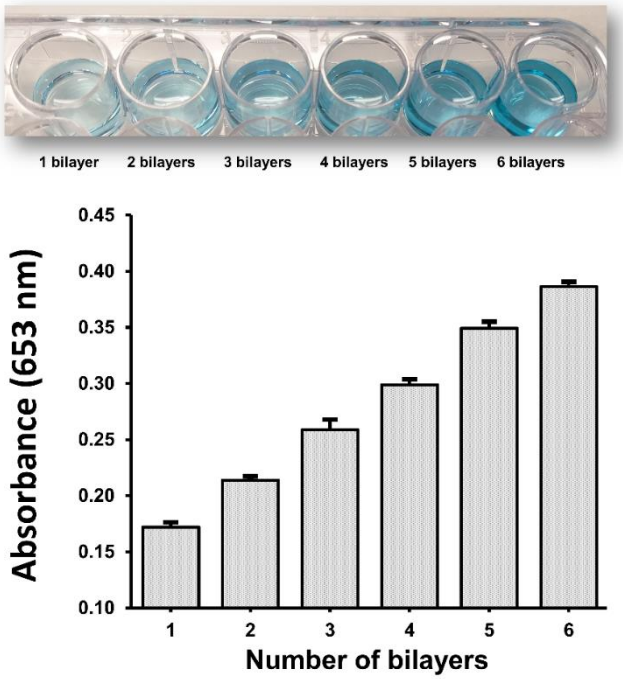

Figure 2-2. Absorbance values at 653 nm for heparin samples dissolved in Taylor's blue dye solution applied to coatings with 1, 2, 3, 4, 5, and 6 bilayers of HEP/COL. Data are presented as the mean ± standard deviation of n = 4samples. Reproduced from [53] with permission from the Royal Society of Chemistry.

Again, an approximate 29% increase in cell viability is observed. Coatings with $(HEP/COL)_6$ demonstrated hSCs with a significant increase in cell viability of up to more than twice above the control. Although $(HEP/COL)_6$ without NGF greatly improves cell behavior, the effect of soluble NGF shows an increase in cell viability of up to 30%. The use of NGF has a considerable impact on the conditions with $(HEP/COL)_6$; suggesting that there is a synergistic action of both components. Also, when the TCPS and $(HEP/COL)_6$ conditions are compared, the fluorescence images showed a huge difference in cell confluence, represented by blue nuclei (see **Figure 2-3A**). The response of hSCs to different surfaces has not been studied extensively; nevertheless,

other studies have obtained similar results. It has been shown that rat Schwann cells can increase their proliferation by up to 130% in implants with titanium or hydroxyapatite coatings without presenting any alteration in their morphology.[14] In a recent study, our group recently demonstrated that human mesenchymal stromal cells (hMSC) showed an increase in their proliferation and protein expression when they were grown in multilayers of HEP/COL supplemented with a cytokine known as interferon-gamma (IFN-γ).[18] Coatings of 5.5 bilayers applied through the LbL method to aligned poly-L-lactide (PLLA) nanofibers were used to encapsulate and release NGF to Schwann cells and PC-12 cells. Both types of cells showed a significant increase in growth, and PC-12 displayer neurite formation in response to NGF.[24] Our coatings may provide a more ideal surface to the hSCs thanks to the presence of the ECM compounds. However, since the PrestoBlue assay is specifically a viability test, which detects only living cells, our results may indicate that either cell adhesion or proliferation –or both– increase when hSCs are in contact with $(HEP/COL)_6$.

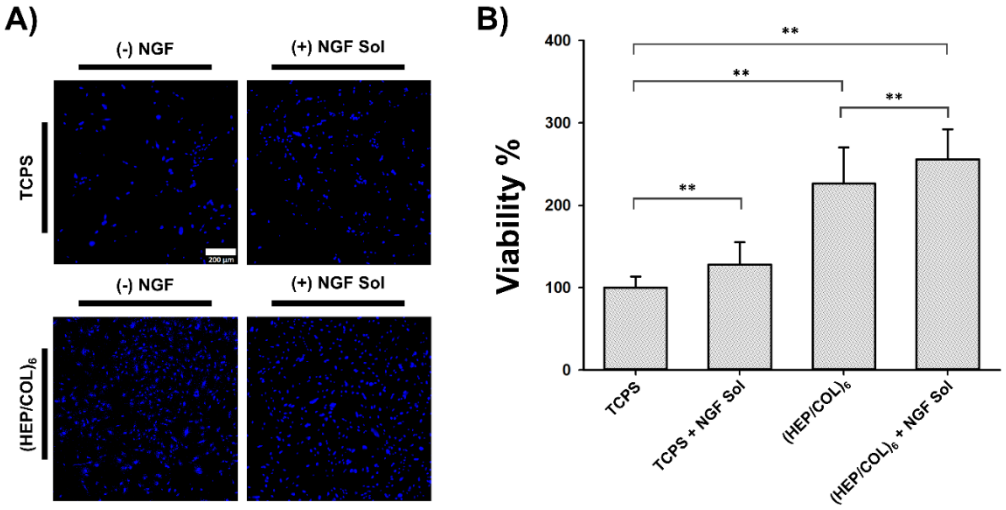

Figure 2-3. PrestoBlue Viability assay for cultured hSCs. (A) Representative fluorescence microscopy images of hSCs nuclei labeled with Hoechst after 6 days of culture. Cellular behavior in cell cultures on TCPS and on $(HEP/COL)_6$ coatings with and without NGF, and (B) viability percentage for hSCs on TCPS and on $(HEP/COL)_6$ coatings with and without NGF after 6 days of culture. Data are presented as the mean $\pm$ standard deviation of n = 8 samples. The p values <0.05 are represented by **. Reproduced from [38] with permission from the Royal Society of Chemistry.

2.3.3 EdU proliferation assay on LbL-Coatings after three days of cell culture

hSCs were labeled with 5-ethynyl-2'-deoxyuridine (EdU) to measure whether the cells have some alteration in the capacity to proliferate under different cell culture conditions. Since EdU binds to the DNA of the cells that are proliferating,[38] EdU is considered as a specific assay for cell proliferation and allows for the determination of if the HEP/COL coatings directly affect proliferation.

After three days of cell culture, we incubated hSCs with EdU for 18 hours. We decided to seed the cells for three days with an initial density of 6250 cells/cm^2, since due to the sensitivity of the method when using this initial number of cells, full confluency was not reached after three days of culture, which allowed for an accurate EdU reading. Followed by the incubation period, the cells were fixed, nuclei were counterstained with Hoechst, and were visualized using fluorescence microscopy. Cells that are positive for EdU show their nuclei stained with a different color (green on **Figure 2-4A**). hSCs were seeded on TCPS with and without NGF added (at 10 ng/mL). TCPS without NGF was treated as the control culture condition. Additionally, hSCs were seeded on $(HEP/COL)_6$ with and without NGF. We determined the percentage of the cells which were positive for EdU in relation to the total amount in the field of view (labeled with DAPI). The results can be seen in **Figure 2-4**. It is not possible to identify an obvious difference in the images of **Figure 2-4A** due to the closeness of the results (between 40 and 47% approximately). After the cell culture period, the exposure to EdU at an equal concentration for all culture conditions showed average results close to 43% of cells positive for EdU. The ANOVA results indicate that there is only a significant difference between the condition with $(HEP/COL)_6$ with NGF and the TCPS control.

$(HEP/COL)_6$ did not alter the ability of hSCs to proliferate even under culture conditions where NGF was not used. After 18 hours with EdU, hSCs showed normal behavior during the incubation time, and the percentage of positive cells for EdU is similar in all conditions compared to the TCPS

culture. We obtained the highest percentage values for culture on $(HEP/COL)_6$ with NGF dissolved in the culture medium, where some trials showed results close to 47% of cells positive for EdU. This finding could be due to the affinity and coupling interactions between heparin and many types of proteins, which could increase the behavior of hSCs by offering a more favorable environment for cell development.[18] Our results suggest that the synergistic combination of $(HEP/COL)_6$ and NGF slightly increase the proliferation of hSCs and, at the same time, show that $(HEP/COL)_6$ favor cell adhesion more than proliferation. However, there is an indirect increase in proliferation since these two factors (proliferation and cell adhesion) are closely related since hSCs are a type of adherent cells.[39] If there is a greater number of cells attached to the surface of the substrate there will be a greater number of cells proliferating. This effect explains why there is no similarity between the results obtained for the viability test with PrestoBlue (**Figure 2-3B**) and the proliferation test with EdU. Additionally, the presence of type I collagen in the coatings can stimulate cell adhesion by activation of integrin receptors, dystroglycan, and N-syndecan, that connect directly to many types of collagen.[40,41] Several researchers previously demonstrated that the incorporation of collagen increases the adhesion and proliferation of MSC, human breast adenocarcinoma cell line, MCF-7, and human cervical adenocarcinoma cell line, HeLa S3.[42,43]

2.3.4 Real-time monitoring of cell behavior and proliferation

To evaluate the real-time behavior related to the hSCs growth, in this study, we cultured hSCs at 25000 cells/cm^2 on $(HEP/COL)_6$ with and without NGF in solution. We also cultured cells on uncovered biosensors as a control surface. The RTCA iCELLigence™ instrument was used to quantify proliferation and analyze real-time cell behavior. RTCA iCELLigence is a system that has biosensors to measure proliferation, viability, migration, and cell growth among several factors. The analysis is achieved through the constant monitoring of the bioelectrical impedance using microchips located in the E-plates microwell.[44]

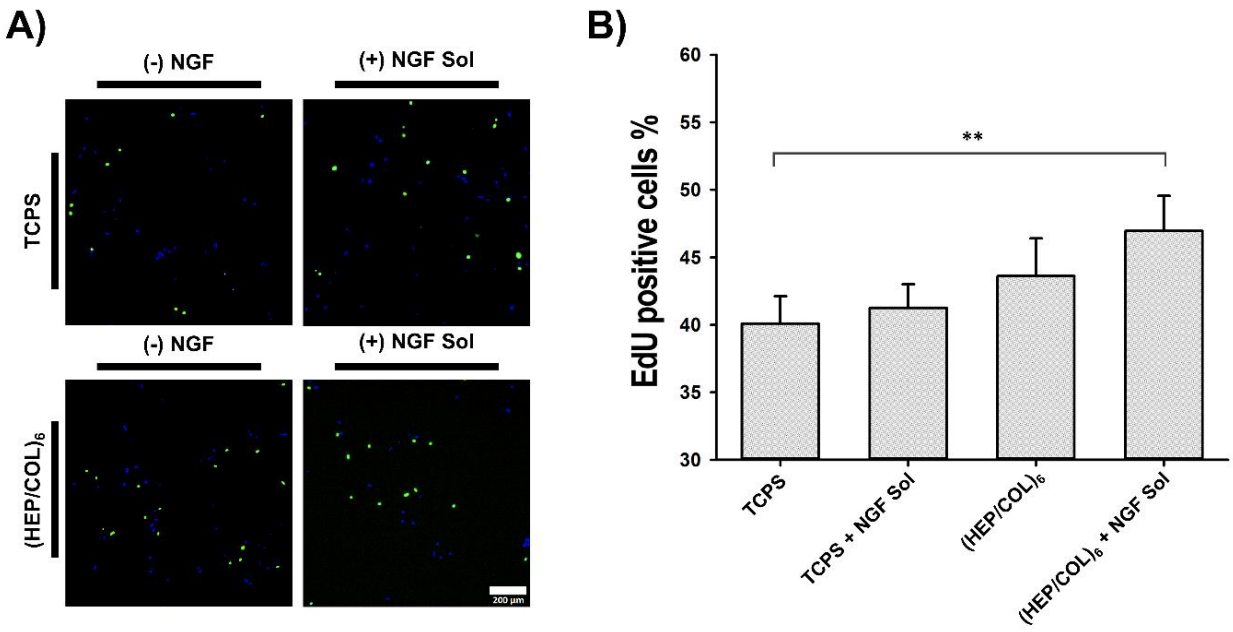

Figure 2-4. Detection of EdU added to cultured hSCs. (A) Representative fluorescence microscopy images of hSCs labeled with EdU Alexa Fluor t 488 and incubated for 18 hours after 3 days of culture (EdU: green; Hoechst: blue). Cellular behavior in cell cultures on TCPS and on (HEP/COL)6 coatings with and without NGF, and (B) percentage of positive cells for EdU on TCPS and on (HEP/COL)6 coatings with and without NGF. Data are presented as the mean ± standard deviation of n = 8 samples. The p values <0.05 are represented by **. Reproduced from [38] with permission from the Royal Society of Chemistry.

This system provides a parameter called Cell Index (CI), which can be used as a measure of proliferation, adhesion, or cytotoxicity. CI at a point *i* is defined as the difference between the background electric resistance (measured using only cell media) Z_0, and the resistance measured at time *t* in the point *i*, Z_i. The CI value is taken at a frequency of 15Ω.[45,46]

CI values are given by the following equation:

$$\boldsymbol{CI = \frac{(Z_i - Z_0)}{15\Omega}} \qquad (1)$$

In **Figure 2-5**, cell index values as a function of time for each of the experimental conditions are shown. We could identify three main regions related to the behavior of Schwann cells.

A first region, between 0 to 30 hours, can be attributed to cell adhesion. A maximum peak is observed near the first 8 to 10 hours, followed by a stabilization period. Compared to the uncoated sensor control, cell adhesion is favored by cultures where $(HEP/COL)_6$ coatings are presented. $(HEP/COL)_6$ in the presence of NGF showed the highest result for CI values during the initial stage of adhesion, suggesting an increase in cell adhesion produced by the joint action of the coatings and NGF in solution. The addition of NGF (at 10 ng/mL) to has been shown to produce increased migratory activity and motility in cell cultures of rat Schwann cells.[47,48] The slope of each curve can be related to the adherence in each culture condition. After 8 hours of culture, a decrease in the slope of all the conditions is observed; this change is attributed to a possible cellular detachment. We obtained similar results when comparing cultures on uncoated sensors with and without NGF. In a range of 80 hours of analysis, an adhesion stage is identified, followed by cell detachment and the beginning of a proliferation stage, and the condition where NGF is used shows higher values for CI (**Figure 2-S3**, appendix).

The second phase, which starts after 30 hours of culture, is attributed to cell proliferation. The beginning of this stage coincides with the doubling time reported by the manufacturer of the cells in the uncovered sensor condition and the $(HEP/COL)_6$ coated sensor without NGF. For the hSCs used in our experiments, the doubling time is 33 hours.[39] During the range between 30 and 90 hours, the culture conditions without NGF show a steady proliferation phase without any decrease in the CI values. The proliferation stage identified for hSCs during this period is consistent with the proliferation results we obtained at a time of three days of cell culture (72 hours), for the EDU test, where about 43% of the cells showed proliferation and the result was similar in the different

conditions (Section 3.3). However, this stage shows an atypical behavior for the condition where $(HEP/COL)_6$ was used with NGF. In this condition, there was almost no proliferation occurring. This performance could be because of the rapid increase in cell adherence observed for this condition in the first 10 hours leading to a confluence close to 100% in a short period. A confluence close to 100% could affect the impedance reading of the microsensors, which is reflected in a straight line with almost no changes. Even so, the range of 50 to 65 hours shows a slight increase in the CI before reaching and maintaining the saturation stage.

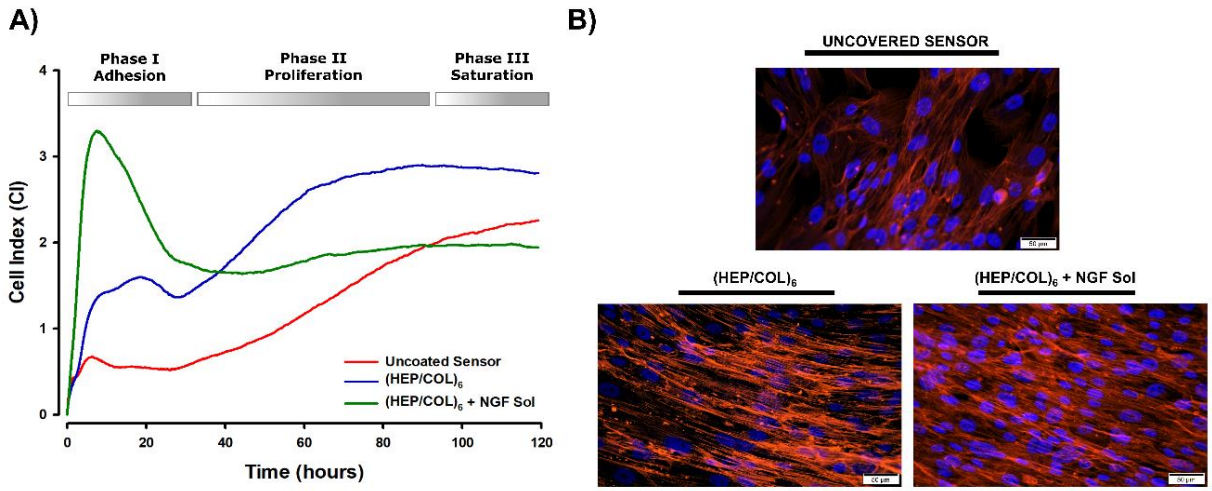

Figure 2-5. Monitoring of real-time hSCs growth on $(HEP/COL)_6$. (A) Cellular behavior on $(HEP/COL)_6$ during 5 days of culture (120 hours), and (B) representative fluorescence microscopy images of hSCs nuclei and actin labeled with Hoechst and Actin Red, respectively, after 5 days of culture. Cellular behavior in cell cultures on TCPS and on $(HEP/COL)_6$ coatings with and without NGF. Reproduced from [38] with permission from the Royal Society of Chemistry.

Finally, the last phase period is between 90 to 120 hours and is the stage in which the growth of the cell stops and stabilizes. This stage can be related to a saturation phase of the biosensors. Several factors can explain this behavior: the cells may have achieved a high confluence (relative to the microwell area), do not have the necessary nutrients to continue growing, or may have the presence of metabolites and cellular secretions that affect cell growth.

The images in **Figure 2-5B** show a complete confluence for cultures on $(HEP/COL)_6$. The conditions with $(HEP/COL)_6$ and NGF may have reached the maximum confluence during the first stage. Maximum confluence can explain the rapid increase in the adhesion stage, with a marked decrease in the CI, followed by a stabilization during the next two phases. Again, we can infer that there is an improvement in the hSCs adhesion for the conditions where $(HEP/COL)_6$ and NGF are used.

2.3.5 Cell morphology and extension

After three days of culture, the hSCs seeded on $(HEP/COL)_6$ remained a normal morphology (bipolar or tripolar spindle shape).[14,33] There are no significant differences in the morphology of cells seeded in TCPS or $(HEP/COL)_6$ (See **Figure 2-6A**). On the other hand, **Figure 2-6B** shows the average cell area of 120 measurements made at each culture condition. Our results showed that the cells seeded in $(HEP/COL)_6$, in the presence of NGF solution, showed a significant increase in their cell extension, close to 1400 μm^2 compared to an average of 1100 μm^2 in the other three conditions. Several factors could explain this particular result. During the regeneration processes, hSCs increase their cell elongation (up to three times the size of standard hSCs) and at the same time express adhesion molecules.[6,13] Also, the addition of NGF greatly increases the production of myelin by the hSCs, which can increase the regenerative functions of the cells.[13,49] Finally, we hypothesize that the increase in cell area may be due to the fact that the (HEP/COL)6 with NGF mimics the native ECM during regeneration. The presence of collagen in our coatings provides binding sites for NGF-activated hSCs, promoting their adhesion and extension.[50]

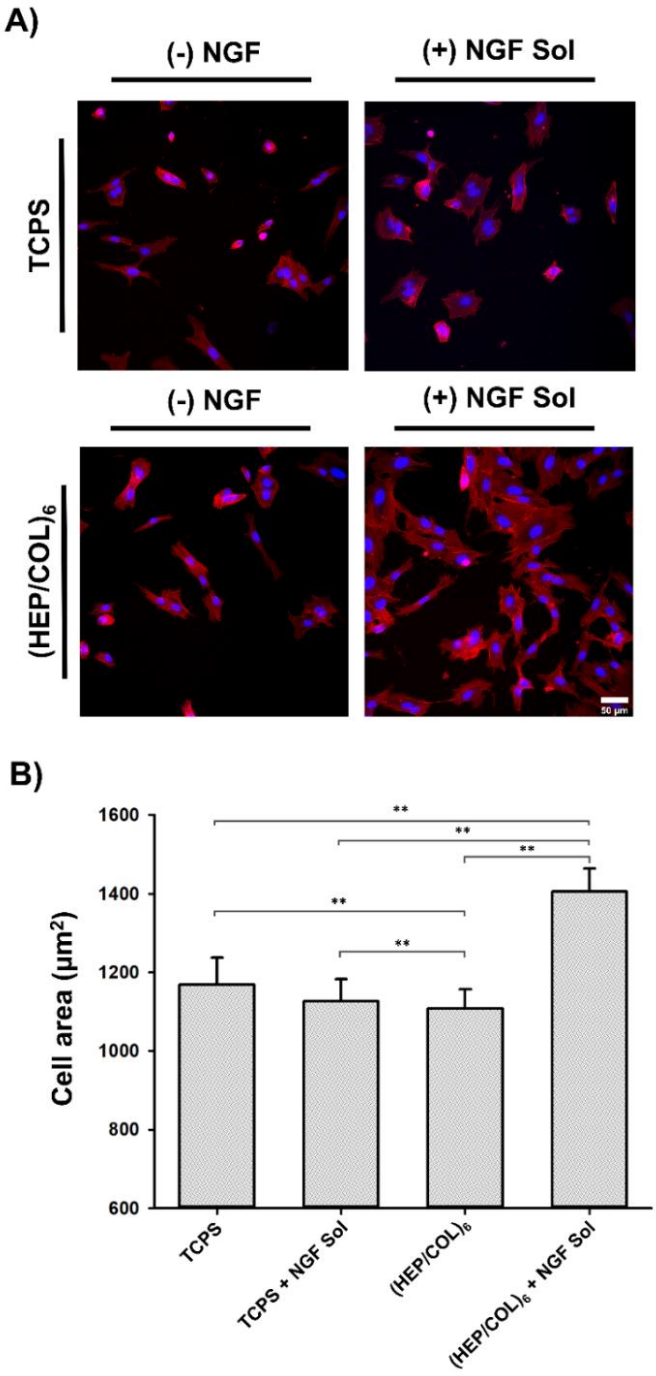

Figure 2-6. Study of morphology and extension of hSCs on (HEP/COL)6. (A) Representative fluorescence microscopic images of hSCs nuclei and actin labeled with Hoechst and Actin Red, respectively, after 3 days of culture. Cellular behavior in cell cultures on TCPS and on (HEP/COL)6 with and without NGF, and (B) average cell area under different cell culture conditions. Data are presented as the mean ± standard deviation of n =120 measurements. The p values <0.05 are represented by **. Reproduced from [38] with permission from the Royal Society of Chemistry.

Additionally, ANOVA analysis shows a significant difference in cell extension for the condition in which hSCs are seeded on $(HEP/COL)_6$ without NGF (See **Figure 2-6B**) when compared to TCPS with and without soluble NGF. We consider that this difference is mostly due to the nature of the method of analysis used. To obtain cell area, 20 cells per image we manually measured. A more robust approach must be used in order to obtain an accurate representation. Nonetheless, our results do consistently show that $(HEP/COL)_6$+NGF yields a larger cell area which might explain the behavior observed in the iCELLigence.

2.3.6 Evaluation of NGF bioactivity using PC-12 cells on $(HEP/COL)_6$

After six days of culture, the morphology of PC-12 cells was normal under all conditions (**Figure 2-7**). The cells showed the small and irregular shape that characterizes them, and there were no differences between the control and the other cultures, and the formation of clusters and agglomerations was evident.[51] In all the conditions where we use NGF, PC-12 cells showed the formation of neurites that corresponds to their transition to neuron-like cells.[33] PC-12 cells are sensitive to NGF when cultured on collagen.[51] This result indicates that $(HEP/COL)_6$ do not alter the response of PC-12 to NGF, indicating that the bioactivity of the NGF is not compromised by the $(HEP/COL)_6$ coatings. On the other hand, it is necessary to pre-treat TCPS surfaces with poly(l-lysine) to achieve the adhesion of PC-12. Poly(l-lysine) allows adhesion due to the charge interaction between the polymer and the cells.[52] This action is replaced by the HEP/COL coatings. Coatings of $(HEP/COL)_6$ promote PC-12 adhesion without the need of PLL.

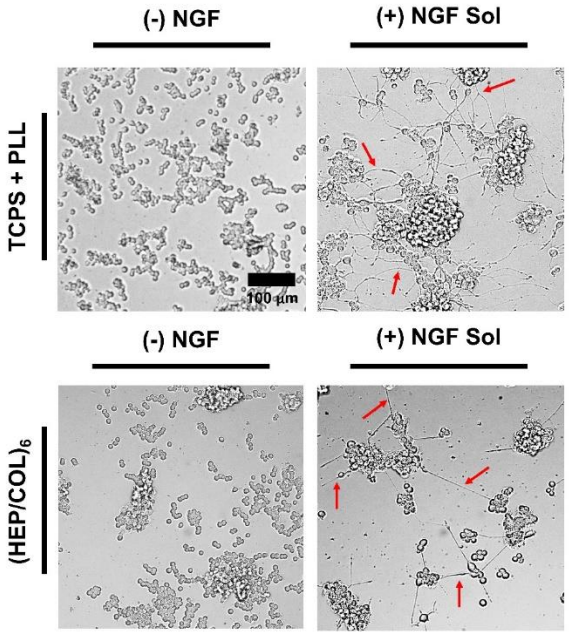

Figure 2-7. Effect of (HEP/COL)6 on the behavior of PC-12 cells. Representative microscopic images of PC-12 cells morphology after 6 days of culture in different conditions: on TCPS with PLL and NGF; and on (HEP/COL)6 with and without NGF in solution. Reproduced from [38] with permission from the Royal Society of Chemistry.

2.4 Conclusion

The LbL technique can be efficiently applied to microwells for cell culture; therefore, it can be used to modify any other surface. Our results showed that: (1) hSCs cultured in HEP/COL coatings showed improved growth compared to TCPS. (2) hSCs cultured in HEP/COL coatings showed an increase in cell number of up to 250% in comparison to cultures in TCPS. (3) The EdU assay revealed that HEP/COL coatings in combination with NGF slightly increases hSCs proliferation and that $(HEP/COL)_6$ greatly promote cell adhesion under different conditions. (4) Real-time monitoring revealed an enhancement in cell adhesion by HEP/COL and HEP/COL coatings with NGF. (5) The morphology of hSCs is not altered in any of the culture conditions since the cells were found in their characteristic form. (6) An increase in the cell area was observed in the condition where $(HEP/COL)_6$ with NGF was used, which suggests that this combination favors cell expansion. And (7) $(HEP/COL)_6$ coatings do not alter the bioactivity of

NGF as evaluated using the PC-12 cells. Therefore, the present study demonstrates that the combination of NGF with HEP/COL coatings further improves hSCs adhesion and expansion. These results are also reflected in an indirect increase of the proliferation thanks to a greater number of cells attached to the substrate surface. Our results showed that HEP/COL coatings could be a useful strategy to improve nerve repair by enhancing human Schwann cell behavior and adhesion. For nerve tissue regeneration, HEP/COL coatings could be a potential application to modify nerve guide conduits to improve their regeneration potential.

2.5 Acknowledgment

This work was funded by the Arkansas Bioscience Institute and the Puerto Rico Idea Network of Biomedical Research Excellence (PRINBRE). Additionally, the authors thank Integra Life Sciences for their generous donation of lyophilized Type I Collagen that was used for this research; ACEA Biosciences for their help with the iCELLigence technology; David Gonzalez-Nino, Dr. Maritza Perez-Perez, Dr. Yu-Hsuan, Chiao, Dr. Ranil Wickramasinghe, Dr. Gary Prinz, and Dr. David Suleiman, for their support with the characterization of the coatings; Kyle Key, John Magness, Claudia Smith and Tyler Merreighn for their collaboration in the experiments for the supplemental information; and Daniel Narváez-Feliciano from the Center for Nanostructure Characterization (CeNaC) at the University of Puerto Rico at Mayaguez for his support with the IRVASE device.

2.6 References

[1] S. Madduri, B. Gander, Schwann cell delivery of neurotrophic factors for peripheral nerve regeneration, Journal of the Peripheral Nervous System. 15 (2010) 93–103. https://doi.org/10.1111/j.1529-8027.2010.00257.x.

[2] S. Ho, P. Labroo, K.M. Lin, S. Himanshu, J. Shea, B. Gale, J. Agarwal, Designing a Novel Drug Delivering Nerve Guide: A Preliminary Study, J Med Biol Eng. 39 (2019) 294–304. https://doi.org/10.1007/s40846-018-0393-y.

[3] L. Tian, M.P. Prabhakaran, S. Ramakrishna, Strategies for regeneration of components of nervous system: scaffolds, cells and biomolecules, Regen Biomater. 2 (2015) 31–45. https://doi.org/10.1093/rb/rbu017.

[4] C.A. Whittaker, K.F. Bergeron, J. Whittle, B.P. Brandhorst, R.D. Burke, R.O. Hynes, The echinoderm adhesome, Dev Biol. 300 (2006) 252–266. https://doi.org/10.1016/j.ydbio.2006.07.044.

[5] B. Pfister, T. Gordon, J.R. Loverde, A.S. Kochar, S.E. Mackinnon, D.K. Cullen, Biomedical Engineering Strategies for Peripheral Nerve Repair: Surgical Applications, State of the Art, and Future Challenges, Crit Rev Biomed Eng. 39 (2011) 81–124. https://doi.org/10.1615/CritRevBiomedEng.v39.i2.20.

[6] P. Arthur-Farraj, K.R. Jessen, Repair Schwann cell update: Adaptive reprogramming, EMT, and stemness in regenerating nerves, Glia. 67 (2019) 421–437. https://doi.org/10.1002/glia.23532.

[7] R. Mirsky, K.R. Jessen, Schwann cell development, differentiation and myelination, Curr Opin Neurobiol. 6 (1996) 89–96. https://doi.org/10.1016/S0959-4388(96)80013-4.

[8] K.R. Jessen, R. Mirsky, The repair Schwann cell and its function in regenerating, J Physiol. 594 (2016) 3521–3531. https://doi.org/10.1113/JP270874.

[9] C. Cheng, D.W. Zochodne, In vivo proliferation, migration and phenotypic changes of Schwann cells in the presence of myelinated fibers, Neuroscience. 115 (2002) 321–329. https://doi.org/10.1016/s0306-4522(02)00291-9.

[10] Y. Wu, L. Wang, B. Guo, Y. Shao, P.X. Ma, Electroactive biodegradable polyurethane significantly enhanced Schwann cells myelin gene expression and neurotrophin secretion for peripheral nerve tissue engineering, Biomaterials. 87 (2016) 18–31. https://doi.org/10.1016/j.biomaterials.2016.02.010.

[11] S.P. Frostick, Q. Yin, G.J. Kemp, Schwann cells, neurotrophic factors, and peripheral nerve regeneration, Microsurgery. 18 (1998) 397–405. https://doi.org/10.1002/(sici)1098-2752(1998)18:7<397::aid-micr2>3.0.co;2-f.

[12] Z.-L. Shen, F. Lassner, M. Becker, G.F. Walter, A. Bader, A. Berger, Viability of cultured nerve grafts: an assessment of proliferation of Schwann cells and fibroblasts, Microsurgery. 19 (1999) 356–363. https://doi.org/10.1002/(sici)1098-2752(1999)19:8<356::aid-micr2>3.0.co;2-n.

[13] E. Mathey, P.J. Armanti, Introduction to the Schwann cell, in: P.J. Armanti (Ed.), The Biology of Schwann Cells: Development, Differentiation and Immunomodulation, Cambridge University Press, Cambridge, 2007: pp. 1–12. https://doi.org/10.1017/cbo9780511541605.

[14] Q. Yuan, D. Liao, X. Yang, X. Li, N. Wei, Z. Tan, P. Gong, Effect of implant surface microtopography on proliferation, neurotrophin secretion, and gene expression of Schwann cells, J Biomed Mater Res A. 93A (2010) 381–388. https://doi.org/10.1002/jbm.a.32548.

[15] P. Lu, V.M. Weaver, Z. Werb, The extracellular matrix: A dynamic niche in cancer progression, J Cell Biol. 196 (2012) 395–406. https://doi.org/10.1083/jcb.201102147.

[16] M.L. Feltri, L. Wrabetz, The role of the extracellular matrix in Schwann cell development and myelination, in: P. Armanti (Ed.), The Biology of Schwann Cells: Development, Differentiation and Immunomodulation, Cambridge University Press, Cambridge, 2007: pp. 55–71. https://doi.org/10.1017/CBO9780511541605.005.

[17] Z. Tang, Y. Wang, P. Podsiadlo, N.A. Kotov, Biomedical Applications of Layer-by-Layer Assembly: From Biomimetics to Tissue Engineering, Advanced Materials. 18 (2006) 3203–3224. https://doi.org/10.1002/adma.200600113.

[18] D.A. Castilla-Casadiego, J.R. García, A.J. García, J. Almodovar, Heparin/collagen coatings improve Human mesenchymal stromal cell response to Interferon Gamma, ACS Biomater Sci Eng. 5 (2019) 2793–2803. https://doi.org/10.1021/acsbiomaterials.9b00008.

[19] P. Gentile, I. Carmagnola, T. Nardo, V. Chiono, Layer-by-layer assembly for biomedical applications in the last decade, Nanotechnology. 26 (2015) 1–21. https://doi.org/10.1088/0957-4484/26/42/422001.

[20] J. Almodóvar, L.W. Place, J. Gogolski, K. Erickson, M.J. Kipper, Layer-by-layer assembly of polysaccharide-based polyelectrolyte multilayers: a spectroscopic study of hydrophilicity, composition, and ion pairing, Biomacromolecules. 12 (2011) 2755–2765. https://doi.org/10.1021/bm200519y.

[21] D.A. Castilla-Casadiego, L. Pinzon-Herrera, M. Perez-Perez, B.A. Quiñones-Colón, D. Suleiman, J. Almodovar, Simultaneous characterization of physical, chemical, and thermal properties of polymeric multilayers using infrared spectroscopic ellipsometry, Colloids and Surfaces A. 553 (2018) 155–168. https://doi.org/10.1016/j.colsurfa.2018.05.052.

[22] Y.N. Sergeeva, T. Huang, O. Felix, What is really driving cell–surface interactions? Layer-by-layer assembled films may help to answer questions concerning cell attachment and response to biomaterials, Biointerphases. 11 (2016) 019009. https://doi.org/10.1116/1.4943046.

[23] S.J. Cifuentes, P. Priyadarshani, D.A. Castilla-Casadiego, L.J. Mortensen, J. Almodóvar, M. Domenech, Heparin/Collagen Surface Coatings Modulate the Growth, Secretome and Morphology of Human Mesenchymal Stromal Cell Response to Interferon-Gamma, J Biomed Mater Res A. (2020). https://doi.org/10.1002/jbm.a.37085.

[24] K. Zhang, D. Huang, Z. Yan, C. Wang, Heparin/collagen encapsulating nerve growth factor multilayers coated aligned PLLA nanofibrous scaffolds for nerve tissue engineering, J Biomed Mater Res A. 105A (2017) 1900–1910. https://doi.org/10.1002/jbm.a.36053.

[25] J. Almodóvar, R. Guillot, C. Monge, J. Vollaire, S. Selimovíc, J.L. Coll, A. Khademhosseini, C. Picart, Spatial patterning of BMP-2 and BMP-7 on biopolymeric films and the guidance of muscle cell fate, Biomaterials. 35 (2014) 3975–3985. https://doi.org/10.1016/j.biomaterials.2014.01.012.

[26] P. Tayalia, D.J. Mooney, Controlled growth factor delivery for tissue engineering, Advanced Materials. 31 (2009) 3269–3285. https://doi.org/10.1002/adma.200900241.

[27] H. Jin, N. Won, B. Ahn, J. Kwag, K. Heo, J. Oh, Y. Sun, S.G. Cho, S. Lee, S. Kim, Quantum dot-engineered M13 virus layer-by-layer composite films for highly selective and sensitive turn-on TNT sensors, Chemical Communications. 49 (2013) 6045–6047. https://doi.org/10.1039/c3cc42032a.

[28] S. Correa, K.Y. Choi, E.C. Dreaden, K. Renggli, A. Shi, L. Gu, K.E. Shopsowitz, M.A. Quadir, E. Ben-akiva, P.T. Hammond, Highly scalable, closed-loop synthesis of drug-loaded, Layer-by-Layer nanoparticles, Adv Funct Mater. 26 (2016) 991–1003. https://doi.org/10.1002/adfm.201504385.

[29] R. Ayala-caminero, L. Pinzón-herrera, C.A. Rivera Martinez, J. Almodovar, Polymeric scaffolds for three-dimensional culture of nerve cells: a model of peripheral nerve regeneration, MRS Commun. 7 (2017) 391–415. https://doi.org/10.1557/mrc.2017.90.

[30] J. Glowacki, S. Mizuno, Collagen scaffolds for tissue engineering, Biopolymers. 89 (2007) 338–344. https://doi.org/10.1002/bip.20871.

[31] S. Klein, J. Vykoukal, O. Felthaus, T. Dienstknecht, L. Prantl, Collagen type I conduits for the regeneration of nerve defects, Materials. 9 (2016) 1–9. https://doi.org/10.3390/ma9040219.

[32] Q. Lin, J. Yan, F. Qiu, X. Song, G. Fu, J. Ji, Heparin/collagen multilayer as a thromboresistant and endothelial favorable coating for intravascular stent, J Biomed Mater Res A. 96 A (2011) 132–141. https://doi.org/10.1002/jbm.a.32820.

[33] S. Geuna, S. Raimondo, F. Fregnan, C. Grothe, In vitro models for peripheral nerve regeneration, European Journal of Neuroscience. 43 (2016) 287–296. https://doi.org/10.1111/ejn.13054.

[34] S. Maniwa, A. Iwata, H. Hirata, M. Ochi, Effects of neurotrophic factors on chemokinesis of Schwann cells in culture, Scand J Plast Reconstr Surg Hand Surg. 37 (2003) 14–17. https://doi.org/10.1080/alp.37.1.14.17.

[35] Y. Uchida, M. Tomonaga, Nerve growth factor accelerates regeneration of cultured adult sympathetic ganglion cells, Age (Omaha). 8 (1985) 19–20. https://doi.org/10.1007/BF02431938.

[36] E.S. Anton, G. Weskampt, L.F. Reichardt, W.D. Matthew, Nerve growth factor and its low-affinity receptor promote Schwann cell migration, Proceedings of the National Academy of Sciences. 91 (1994) 2795–2799. https://doi.org/10.1073/pnas.91.7.2795.

[37] A.M. Ferreira, P. Gentile, S. Toumpaniari, G. Ciardelli, M.A. Birch, Impact of Collagen/Heparin multilayers for regulating bone cellular functions, ACS Appl Mater Interfaces. 8 (2016) 29923–29932. https://doi.org/10.1021/acsami.6b09241.

[38] A. Salic, T.J. Mitchison, A chemical method for fast and sensitive detection of DNA synthesis in vivo, Proceedings of the National Academy of Sciences. 105 (2007) 2415–2420. https://doi.org/10.1073/pnas.0712168105.

[39] ATCC USA, Product sheet for sNF96.2 (ATCC® CRL-2884™), (1994) 1–2. https://www.atcc.org/~/ps/CRL-2884.ashx (accessed October 2, 2019).

[40] J. Heino, The collagen family members as cell adhesion proteins, BioEssays. 29 (2007) 1001–1010. https://doi.org/10.1002/bies.20636.

[41] J.A. Weiner, N. Fukushima, J.J.A. Contos, S.S. Scherer, J. Chun, Regulation of Schwann Cell Morphology and Adhesion by Receptor-Mediated Lysophosphatidic Acid Signaling, 21 (2001) 7069–7078.

[42] M.F. Najafi, F. Vahedi, S. Ahmadi, R. Madani, M. Mehrvarz, Effect of Collagen type I (rat tail) on cell proliferation and adhesion of BHK-21, in: 4th Kuala Lumpur International Conference on Biomedical Engineering 2008, Springer Berlin Heidelberg, 2008: pp. 806–809. https://doi.org/10.1007/978-3-540-69139-6_200.

[43] C. Somaiah, A. Kumar, D. Mawrie, A. Sharma, S.D. Patil, J. Bhattacharyya, R. Swaminathan, B.G. Jaganathan, Collagen promotes higher adhesion, survival and proliferation of Mesenchymal stem cells, PLoS One. 10 (2015) 1–15. https://doi.org/10.1371/journal.pone.0145068.

[44] J. Stefanowicz-Hajduk, A. Adamska, R. Bartoszewski, J.R. Ochocka, Reuse of E-plate cell sensor arrays in the xCELLigence real-time cell analyzer, Biotechniques. 61 (2016) 117–122. https://doi.org/10.2144/000114450.

[45] ACEA Biosciences Inc., xCELLigence ® RTCA S16 Operator's Manual, 2nd ed., ACEA Biosciences, Inc., San Diego, 2018.

[46] ACEA Biosciences Inc. USA, The xCELLigence system, (2013) 1–20. https://www.aceabio.com/wp-content/uploads/xCELLigence-RTCA-SP-MP-Instruments.pdf (accessed October 22, 2019).

[47] S. Maniwa, A. Iwata, H. Hirata, M. Ochi, Effects of neurotrophic factors on chemokinesis of Schwann cells in culture, Scand J Plast Reconstr Surg Hand Surg. 37 (2003) 14–17. https://doi.org/10.1080/alp.37.1.14.17.

[48] E.S. Anton, G. Weskampt, L.F. Reichardt, W.D. Matthew, Nerve growth factor and its low-affinity receptor promote Schwann cell migration, Proceedings of the National Academy of Sciences. 91 (1994) 2795–2799. https://doi.org/10.1073/pnas.91.7.2795.

[49] J.R. Chan, T.A. Watkins, J.M. Cosgaya, C. Zhang, L. Chen, L.F. Reichardt, E.M. Shooter, B.A. Barres, NGF controls axonal receptivity to myelination by Schwann cells or oligodendrocytes, Neuron. 43 (2004) 183–191. https://doi.org/10.1016/j.neuron.2004.06.024.

[50] S.G.A. Van Neerven, L. Krings, K. Haastert-Talini, M. Vogt, R.H. Tolba, G. Brook, N. Pallua, A. Bozkurt, Human Schwann cells seeded on a novel collagen-based microstructured nerve guide survive, proliferate, and modify neurite outgrowth, Biomed Res Int. 2014 (2014) 1–13. https://doi.org/10.1155/2014/493823.

[51] ATCC USA, Product sheet for PC-12 (ATCC® CRL1721™), (2018) 1–3. https://www.atcc.org/~/ps/CRL-1721.ashx (accessed October 14, 2019).

[52] D. Mazia, G. Schatten, W. Sale, Adhesion of Cells to Surfaces Coated with Polylysine, Journal of Cell Biology. 66 (1975) 198–200. https://doi.org/10.1083/jcb.66.1.198.

[53] L. Pinzon-Herrera, J. Mendez-Vega, A. Mulero-Russe, D.A. Castilla-Casadiego, J. Almodovar, Real-time monitoring of human Schwann cells on heparin-collagen coatings reveals enhanced adhesion and growth factor response, J Mater Chem B. 8 (2020) 8809–8819. https://doi.org/10.1039/d0tb01454k.

CHAPTER 3. Heparin-collagen layer-by-layer coatings improve protein expression potential and cell migration in human Schwann cells: stability studies and application to a commercial Nerve guide conduit.

3.1 Abstract

In this work, we studied the enhancing effect of six bilayers of heparin/collagen $(HEP/COL)_6$ layer-by-layer coatings on human Schwann cell (hSCs) protein expression and cell migration in the presence or absence of nerve growth factor (NGF). $(HEP/COL)_6$ stability and in vitro bioactivity effects were also studied during 28 days after incubating the coatings with cell culture medium. Finally, $(HEP/COL)_6$ was applied to a commercial collagen-based nerve guide conduit, NeuraGen®, and the hSCs viability was studied after 6 days of cell culture on the coated implants. hSCs cultured in $(HEP/COL)_6$ showed an improved protein expression potential, and our coatings greatly promote hSCs migration. $(HEP/COL)_6$ was very stable up to 21 days after incubation with cell media before the cell seeding showing an increased viability. Finally, the morphology of NeuraGen® is not altered by the action of $(HEP/COL)_6$, and an increase in the cell viability was observed in the condition where NeuraGen® with $(HEP/COL)_6$ was used.

3.2 Introduction

Peripheral nerve injury (PNI) is defined as damage to peripheral nerve tissue that results in its malfunction.[1] Most often PNIs are the result of physical trauma, genetic factors, or immune diseases.[2] The annual estimate for medical expenses exceeds 150 billion, with an average of more than 550,000 surgeries in the US caused by PNIs.[3,4] The gold standard for PNI repair is autograft surgery. In this process, healthy tissue is extracted from the patient and implanted in the lesion.[5] Autograft implantation can cause loss of function at the donor site, infection,

scarring, or even the need for additional surgeries.[3,6,7] As a result of this, there is a need to find strategies aimed at solving this clinical problem.

Nerve guide conduits (NGCs), which are currently approved for clinical use in the treatment of PNI, have emerged in recent years as possible substitutes for the use of autografts.[8] However, the challenge is to repair large gaps using NGCs, this being possible only if the implant improves the interactions between the cells and the extracellular matrix (ECM).[8,9] The limitation of using NGCs is that they are able to repair short lesions of less than 1 cm, due to the lack of components present in the ECM that can be found in autografts.[8]

When PNI occurs, human Schwann cells (hSCs) are activated to facilitate an important collaboration between macrophages and neurons, and additionally they promote and support tissue repair.[10] In this sense, these cells adopt a genotype known as Repair Schwann Cells.[11] Therefore, it is important to improve hSCs properties such as cell adhesion, proliferation, migration, and protein expression.

To target this aim, this research looks for the creation of a novel and enhanced implant, by modifying the surface of a commercial NGC using layer-by layer coatings with natural polymers. The coatings will be composed of *6 bilayers composed of heparin (HEP) and collagen (COL)*, which from this point on will be noted as $(HEP/COL)_6$. Making the coatings with HEP/COL, both natural polymers widely present in the ECM, will offer mimetic properties that will decrease the immune response of NGCs. HEP and COL will provide a high affinity for drugs or proteins, and supporting and structural properties, respectively.[12,13] The resulting NGC will improve cell behavior and will be highly adaptable, since an important complement when using NGCs is the

presence of growth factors (GFs) such as the Nerve growth factor (NGF) or Brain derived neurotrophic factor (BDNF).[14]

Therefore, this research aims to study hSCs behavior in vitro in terms of cell migration, and protein expression on Tissue culture Polystyrene (TCPS), and the cell adhesion and proliferation when cultured on NGCs modified by the layer-by-layer method with coatings using $(HEP/COL)_6$. The effect of NGF is also considered by the addition of this protein to the cell media. The stability of $(HEP/COL)_6$ will be studied by incubating the coatings during 30 days before sending the cells.

3.3 Materials and methods

3.3.1 Cell Culture and experimental conditions

Human Schwann cells (hSCs) from ATCC® (sNF96.2 ATCCs CRL-2884^{TM}), from a 28-year-old male, were used between passages 17 to 20, and grown in Dulbecco's Modified Eagle's Medium from SIGMA-ALDRICH® (Cat. #D5648) containing 10% Fetal bovine serum from Gibco® (Cat. #10-437-028), 1% Penicillin–streptomycin from SIGMA-ALDRICH® (Cat. #P4333) and supplemented with sodium bicarbonate and sodium pyruvate. The cells were incubated in a humid incubator at 37 °C with an air atmosphere containing 5% CO_2. These culture conditions are similar to those used in our previous work.[15]

The parameters resulting from this research were evaluated under two conditions: on $(HEP/COL)_6$ and on $(HEP/COL)_6$ with recombinant human beta nerve growth factor (NGF) from R&D Systems (Cat. #256-GF/CF) at a concentration of 10 ng/mL dissolved in the culture medium.[16–18] Two controls, on TCPS or uncoated NGCs, with and without NGF were also used.

3.3.2 $(HEP/COL)_6$ construction on well plates and on NGCs using the Layer-by-layer method

The traditional layer-by-layer dipping method was used to fabricate $(HEP/COL)_6$ on NGCs. In contrast, a variation of the technique was used to perform coatings to cell culture plates by adding polyelectrolyte solutions to each well (**Figure 3-1**). However, the basics of both methods are the same and described in our previous works.[15,19] Briefly, poly-(ethylene imine) (PEI) (50% solution in water, Mw ≈ 750,000) from Sigma-Aldrich (Cat. # P3143), sodium heparin produced by Smithfield Bioscience, Inc. (Cat. # PH3005) and Lyophilized type I collagen sponges (generously donated by Integra Lifesciences Holdings Corporation, Añasco, PR), were used to prepare polymer solutions. Polymer solutions were prepared at a concentration of 1.0 mg/mL in sodium acetate buffer (at pH=5 for HEP and PEI, and pH=4 for COL). We used ultra-pure water at 18.2 MΩ-cm to prepare solutions and as the washing solution, sodium acetate buffer at pH=5 and. The procedure was carried out as follows: samples were pre-treated, either wells or NGCs, by adding PEI solution for 15 minutes, followed by a 3-minute wash. This pretreatment was performed to produce a highly positive anchor layer before applying the HEP/COL coatings. After this, HEP and COL solutions were deposited for 5 minutes alternating with an intermediate wash of 3 minutes. This procedure is done to form one bilayer and was repeated in a total of 6 times to reach $(HEP/COL)_6$. As final steps, a wash was performed with sterile DI water and another with phosphate-buffered saline (PBS 1X) from ThermoScientific™ (Cat. # 28372) for 3 minutes each. NGC samples were left to dry overnight. A UV sterilization step was performed for 10 minutes before cell culture.

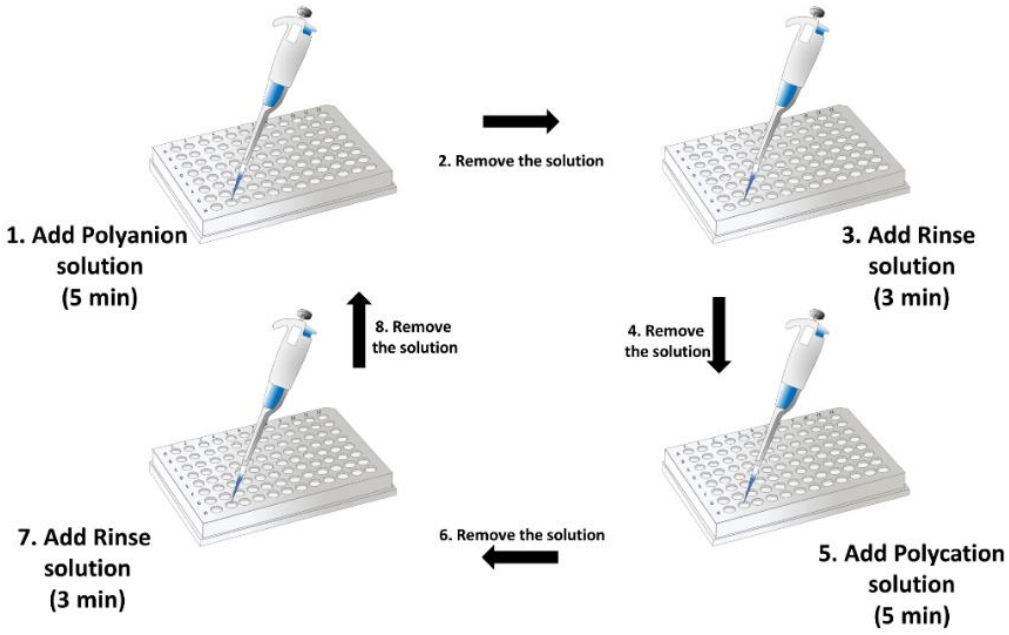

Figure 3-1. Scheme of LBL method applied by adding and removing the polymeric solutions to a cell culture plate to create coatings on the bottom of the wells.

3.3.3 hSCs protein expression on $(HEP/COL)_6$

Protein determination, for a total of 12 analytes, was performed with a Luminex MAGPIX® and using two Invitrogen kits: ProcartaPlex 5 PLEX PPX05 (Assay ID: MXYMKUE) and Human ProcartaPlex PPX07 (Assay ID: MXXGR9G). Briefly, cells were seeded at a density of 30000 cells/cm^2 in wells of 24-Well Corning™ Costar™ flat-bottom polystyrene microplates (Fisher Cat. # 07-200-740, area of 1.9 cm^2/well), and after 3 and 6 days of culture, samples of 500 µL of the supernatant culture medium were taken. These samples were then stored in a freezer at -80°C. On the analysis day, the samples were slowly thawed on ice, vortexed, and centrifuged at 2000 *g* for 1 minute. After this step, 50 µL of each sample was analyzed according to the protocol established by each kit.

3.3.4 hSCs migration on $(HEP/COL)_6$

In vitro cell migration was evaluated with a circular barrier–based assay. A 3D model with a 2 mm diameter circular tip was designed using SketchUp 2020 software and printed on the 3D printer owned by the Ralph E. Martin Department of Chemical Engineering at the University of Arkansas. Red Polyacrylonitrile-butadiene-styrene (ABS) from Push Plastic (d = 2.85 mm) was used for the plastic models. The barriers were inserted into wells of 24-Well Corning™ Costar™ polystyrene microplates previously coated with $(HEP/COL)_6$. hSCs were seeded at a density of 100,000 cells/cm^2, allowing cells to adhere to the entire bottom of the well and around the circular barrier. After three days of incubation, the barrier was removed, and the cell-free area was left exposed. Monitoring with photographs will be done every 5 to 10 hours. Migration was determined in terms of the area covered by the cells over time. ImageJ software will allow you to measure the area covered in each photo.

3.3.5 $(HEP/COL)_6$ stability studies

Stability assays were carried out by studying the effects of cell medium over time on TCPS and ACEA™ E-Plates 16, covered with $(HEP/COL)_6$. We evaluated the cell proliferation and adhesion and, simultaneously, the real-time cell behavior of human Schwann cells during and after three days of culture on coated microwells. Coatings were performed on five plates of each type, then 4 of those were subjected to incubation with 200 µl of cell culture medium over the coatings (the incubation periods are shown in **Table 3-1**). Incubation was done after storage without shaking inside an incubator at 37°C and in an environment with 5% CO2. After each incubation period, the cell medium was removed, and the cells were seeded on the plates at 25,000 cells/cm2. As in previous experiments, hSCs growth was also evaluated under two different conditions on

$(HEP/COL)_6$, and $(HEP/COL)_6$ with NGF at 10 ng/mL, and the results were compared with two controls: uncovered wells with and without NGF.

Table 3-1. Incubation time for plates used in stability studies

Plate No.	Incubation time
1	0 hours*
2	7 days
3	14 days
4	21 days
5	28 days

*Cells seeded immediately the coatings are applied

3.3.5.1 Effect of the (HEP/COL)6 age on the hSCs viability

$(HEP/COL)_6$ was constructed on the wells of five on Corning™ 3603 96-Well clear bottom black polystyrene microplates (Fisher Cat. # 07-200-565, cell growth area of 0.32 cm² per well), and PrestoBlue™ cell viability reagent from Invitrogen (Cat. # A13261) were used for this analysis. We followed the directions detailed in **Section 3.3.5** and after 3 days of culture, the medium was removed, and 100 µL of a mixture containing 90 % of fresh culture medium with 10% of PrestoBlue™ Reagent was added. The cells were incubated for 3 hours, and the fluorescence intensity measurement was determined with a BioTek Multi-Mode Microplate Reader (Model Synergy™ 2) with excitation/emission of 560/590 nm.

3.3.5.2 Effect of the (HEP/COL)6 age on the hSCs real-time behavior

$(HEP/COL)_6$ was constructed on the wells of five ACEA™ E-Plate 16 (Cat. # 05469830001, cell growth area of 0.19 cm² per well), and a Real-Time Cell Analyzer S16 (RTCA) xCELLigence instrument from ACEA Biosciences Inc. (Cat. # 00380601430) was used to measure real-time cell behavior for 3 days. We followed the directions detailed in **Section 3.3.5** and monitored the

cell behavior for 3 days of culture. The readings of cell attachment were done every 10 minutes.[15]

3.3.5.3 Cumulative heparin release assays from $(HEP/COL)_6$

To determine the cumulative release of heparin from the coatings, we prepared (HEP/COL)6 in 8 wells in two different 24-Well Corning™ Costar™ polystyrene microplates, one for the tests with PBS and another for the cell culture medium. We add 1mL of PBS or culture medium to each well (Plate #1, only PBS; and Plate #2, only cell medium). Both plates were placed inside the incubator for 30 days (37°C and CO2 at 5%). Sampling corresponded to 1 mL of the supernatant and was taken every 72 hours for 30 days. Quantification of heparin in the collected supernatant was determined by preparing and measuring the absorbance of a mixture of 50 µL of each sample with 50 µL of Azure A solution (80 µg/mL). The results were translated into heparin concentration values when compared to a calibration curve prepared according to the method for heparin quantification described by Warttinger, et al.16 Briefly, sodium heparin standards were prepared in PBS and in cell medium at concentration values of 0, 5, 10, 15, 20, 30, and 40 ng/mL. Then, 50 µL of each standard was mixed with 50 µL of Azure A solution, and the mixture was placed in a 96-well Corning™ Costar™ flat-bottom polystyrene microplate (Fisher Cat. # 07-200-87). Standards and samples were analyzed in triplicate on a BioTek Multi-Mode Microplate Reader (Model SynergyTM 2) at a wavelength of 630 nm.

3.3.6 Surface deposition of $(HEP/COL)_6$ on a commercial NGC

$(HEP/COL)_6$ was carried out on the NeuraGen® from Integra LifeScience Corporation (Cat. # PNG330) surface applying traditional layer-by-layer dipping method described in **Section 3.3.2**. To qualitatively demonstrate heparin deposition due to $(HEP/COL)_6$, a colorimetric test will be performed with Azure A reagent from Thermo Scientific™ (Cat. # AAJ6134614). For this, an 80

µg/mL solution of Azure A was prepared in deionized water, and a 200ul of solution was applied to the NGC samples with and without $(HEP/COL)_6$. Azure A solution is blue and turns purple in the presence of heparin.[20] The morphology of NGCs samples, with and without $(HEP/COL)_6$, was assessed by Scanning Electron Microscopy (SEM).[19]

3.3.7 hSCs viability and adhesion on coated NGCs

Small circles of NGCs (d = 6 mm), with and without $(HEP/COL)_{6,}$ were cut and then placed in the wells of a Corning™ 3603 96-Well clear bottom black polystyrene microplates (Fisher Cat. # 07-200-565, cell growth area of 0.32 cm^2 per well). hSCs were seeded with a cell density of 31,250 cells/cm^2, with a 15-minute incubation period at room temperature with prior incubation to complete the necessary volume of culture medium and NGF solution. Cell viability studies were carried out after six days of culture, using the PretoBlue™ reagent and following the instructions described in **Session 3.3.5.1**. Cell adhesion was carried out by fluorescence imaging by subjecting the samples to the Hoechst 33342 and Actin Red staining protocol (see **next section**).

3.3.8 Immunofluorescence staining

Cellular staining was performed with the fluorescent blue dye from Hoechst 33342 from Invitrogen (Ref. # H3570), which stains the cell nucleus. A Leica inverted fluorescence microscope was used to capture images of cells over NGCs, with standard DAPI filter (excitation/emission of 350/461 nm) to detect Hoechst 33342.

3.4 Results and Discussion

3.4.1 Effect of $(HEP/COL)_6$ on hSCs protein expression potential

A total of 12 analytes were determined for the protein expression study. The panel includes some proteins involved in cell proliferation, differentiation, growth, migration, and adhesion. Similarly, proteins related to the Schwann cell myelination process and cytokines that regulate the pro and anti-inflammatory response are included. **Table 3-2** shows the list of analyzed analytes as well as their functions.

Table 3-2. List of analytes quantitatively determined in this study and their functions.

No.	***Protein Name***	***Abbreviation***	***Function***
1	Fibroblast Growth Factor 2	FGF-2	Contribute to the proliferation and differentiation on different types of cells.[21]
2	Vascular Endothelial Growth Factor A	VEGF-A	Acts specifically on endothelial cells regulating permeability, differentiation, growth, and migration.[22]
3	Hepatocyte Growth Factor	HGF	Regulate cell growth, cell motility and tissue regeneration.[23]
4	Tumor Necrosis Factor α	TNF alpha	Mediator of inflammatory and immune functions. Regulate growth and differentiation.[24,25]
5	Transforming Growth Factor beta 1	TGF beta 1	Inflammatory and immune functions. Contribute to the proliferation and differentiation on different types of cells. Regulates many other growth factors.[26]
6	Interleukin 8	IL-8 (CXCL8)	Protein involved in the chemotaxis and activation of neutrophils.[27]
7	Interleukin 10	IL-10	Related to anti-inflammatory response.[25] IL-10 inhibits the expression of proinflammatory cytokines such as IL-1 and TNF-α.[28]
8	Brain Derived Neurotrophic Factor	BDNF	Promote both the timing and extent of myelination in vitro.[29]
9	S100 proteins A8 & A9	S100 A8/A9	Protein suppressed during myelination.[30]
10	Vascular Endothelial Growth Factor D	VEGF-D	Promotes the growth and remodeling of blood vessels and lymphatic vessels[31]. Regulates tumor progression. Its over expression induces changes in the morphology of fibroblasts.[32]
11	Nerve Growth Factor beta	NGF-beta	Provides essential signals for neuronal survival and repair.[33] Increases cell adhesion.[16,18]
12	Glial Cell line-derived Neurotrophic Factor	GDNF	Promote both the timing and extent of myelination in vitro.[29] Promotes the differentiation and survival of neurons in vitro.[34]

Figure 3-2 shows a heat map format of the results for each analyte concerning the calculated Z-score (from -1.5 to 1.5). Eight samples were analyzed per condition for hSCs cultured for 3 and 6 days.

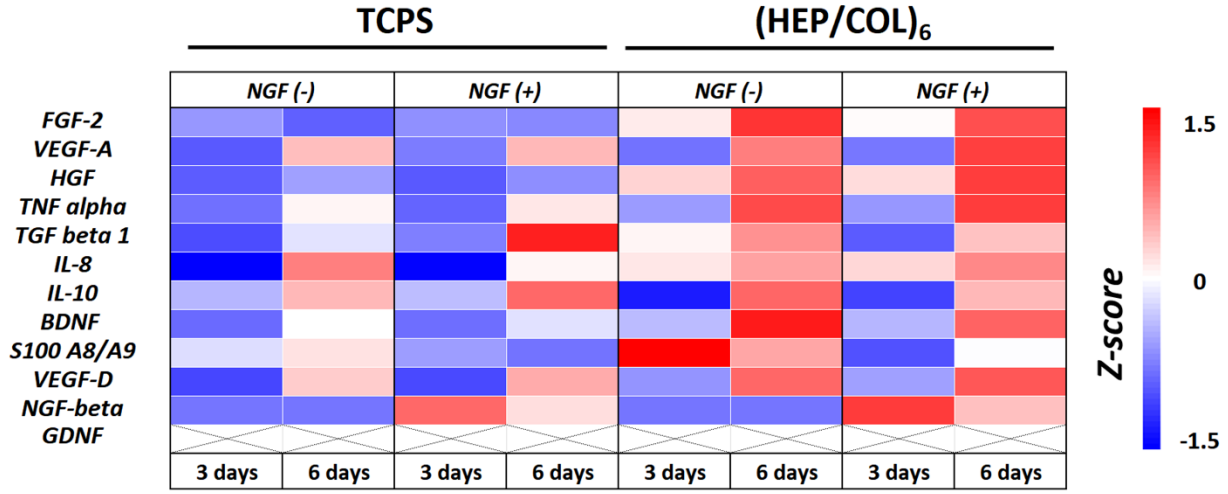

Figure 3-2. hSCs protein expression potential as a response of 3 and 6 days of cell culture on $(HEP/COL)_6$. Heatmap shows the Z-score values of 11 human proteins. Data is presented as the mean of n = 8 samples.

Most of the proteins, compared to controls, had a higher secreted concentration on $(HEP/COL)_6$ with and without NGF added to the cell culture.[35] FGF-2 expression was slightly upregulated by $(HEP/COL)_6$, and the increase was maintained from 3 to 6 days of culture even if NGF was not used. In contrast, FGF-2 expression remained constant under the TCPS conditions. Again, the concentration of VEGF-A, HGF, THF Alpha, VEGF-D, and TGF beta 1, increased enormously for the six days of culture in all culture conditions, being the highest results in $(HEP/COL)_6$, where the increase in the secretion was approximately 1.5-fold higher compared to controls. NGF stimulation favors the expression of VEGF-A and HGF. The secretion of IL-8 and IL-10 is not significantly affected by $(HEP/COL)_6$ or the addition of NGF to the culture medium. We were able

to determine that there is an increase in the concentration of these cytokines in all conditions, showing constant values in the results of 3 and 6 days, respectively.

Figure 3-3 shows the results for the concentration of BDNF (pg/ml) expressed by hSCs. Interestingly, for BDNF, we found the highest increase relationship, which is an exciting finding since this protein is widely related to the myelination process of hSCs.[29] We also observed that the concentration of BDNF improved in all conditions when comparing the samples taken at 3 and 6 days. However, our coatings exert a favorable effect on BDNF expression by raising its concentration by 360% for $(HEP/COL)_6$ without NGF and 305% for $(HEP/COL)_6$ with NGF after 6 days.

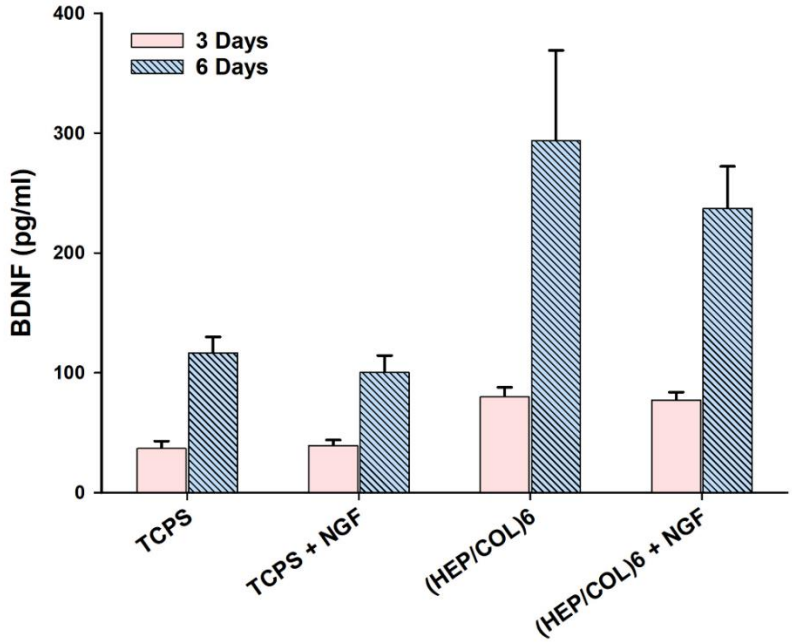

Figure 3-3. hSCs expression of BDNF in response to 3 and 6 days of cell culture in $(HEP/COL)_6$. Data are presented as the mean ± standard deviation of n = 8 samples.

S100 proteins analysis showed a 6% decrease in the samples corresponding to 6 days of cell culture on TCPS with NGF and, surprisingly, 22% on $(HEP/COL)_6$ without NGF. It has been previously shown that the expression of S100 A8/A9 proteins are suppressed during the

myelination process.[30] Therefore, this considerable decrease is another crucial finding attributed to a favorable use of $(HEP/COL)_6$.

When studying NGF external effects in some of the conditions, the analysis for this growth factor is a little different. The conditions where NGF was not added to the culture medium showed 6 and 12 pg/ml for the samples of 3 and 6 days, respectively (50% increase). In contrast, for TCPS and $(HEP/COL)_6$ with NGF, a 50% reduction in the final concentration was obtained since the results were close to 4000 and 2000 pg/ml for 3 and 6 days, respectively. Considering that the initial concentration used for NGF at cell seeding was 10,000 pg/ml (10 ng/ml), the decrease in this protein is mainly attributed to its degradation over time or the effects due to the presence of hSCs.

Finally, GDNF was not detected since it is possible that the cells did not secrete this protein, or its levels in the samples were much lower than the kit detection limit (58.2 pg/ml). This result may be because GDNF expression is increased dramatically under specifically controlled culture conditions of SCs,[36] and it is also widely known that GDNF is one of the neurotrophic factors whose expression is increased after a peripheral nerve injury.[37]

3.4.2 hSCs migration to $(HEP/COL)_6$

Figure 3-4 summarizes the results obtained in a circular barrier–based migration assay. We designed and printed a 3D model with a circular tip with a 2 mm diameter (**Figure 3-4B**). The device was placed in contact with the bottom of the wells with or without $(HEP/COL)_6$. For this experiment, a high density of cells was seeded and allowed to grow around the circular barrier. Once 100% cell confluency was around the tip (approximately after three days of culture), the device was removed, and the hSCs were allowed to migrate to the cell-free area. How the cells covered the cleared area was monitored by taking pictures every 5 to 10 hours for a total of 70 hours. The covered area was determined on each photo using ImageJ (see **Figure 3-4C**).

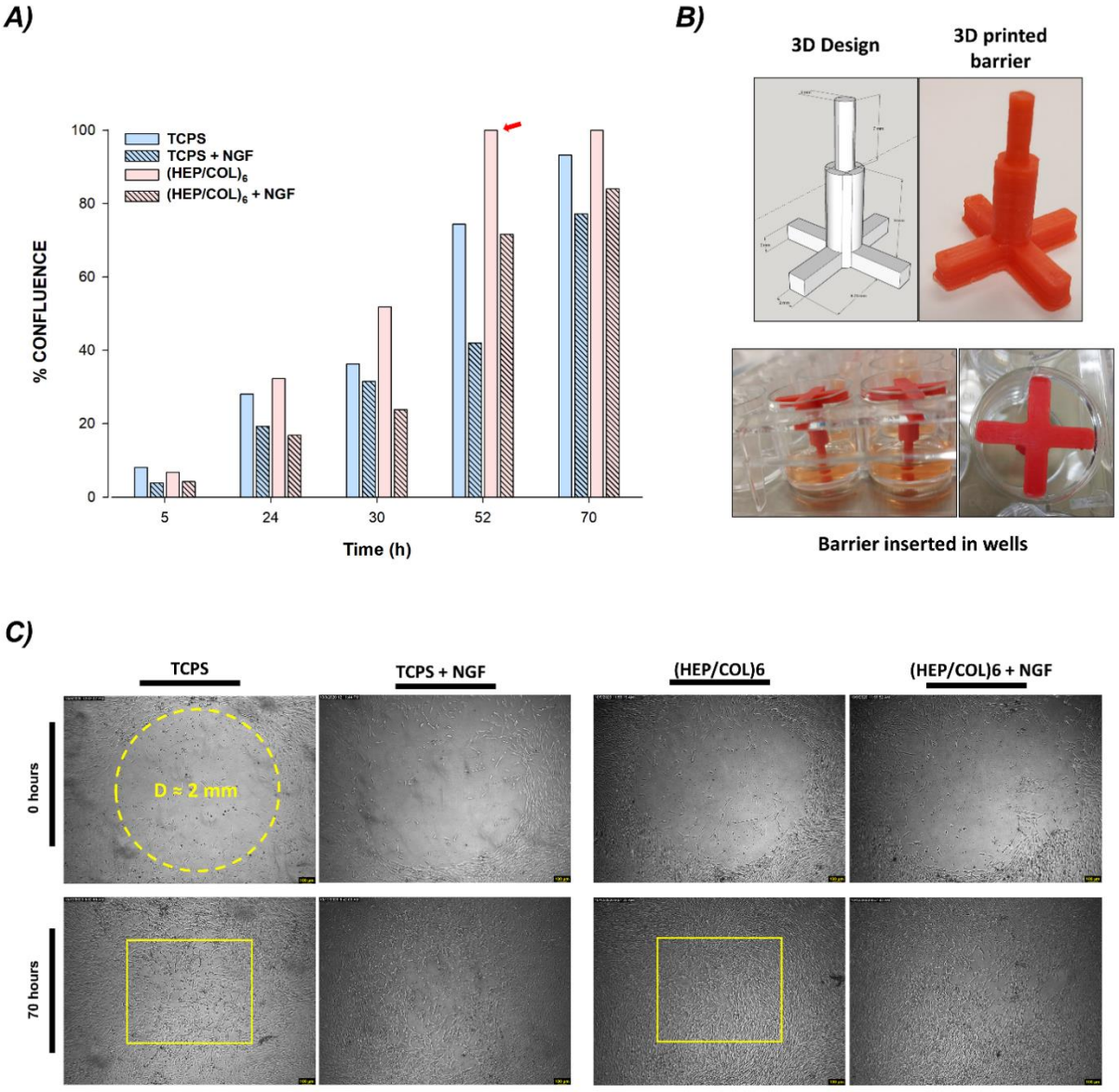

Figure 3-4. hSCs migration experiment to cover a circular diameter of 2 mm. (A) Area coverage percentage for hSCs from 5 to 70 hours of cell culture in different conditions: on TCPS with and without NGF; and on $(HEP/COL)_6$ with and without NGF in solution, (B) 3D printed barrier used in this experiment; and (C) Representative microscopic images of hSCs morphology after 70 hours of culture in different conditions: on TCPS with and without NGF; and on $(HEP/COL)_6$ with and without NGF in solution.

The bar graph in **Figure 3.4A** shows the hSCs confluence percentage towards the cell-free area from 5 to 70 hours. Surprisingly, $(HEP/COL)_6$ obtained the best results. After 52 hours, the hSCs migrated into the coatings and reached 100% confluency (red arrow), whereas, by the same time, TCPS, $(HEP/COL)_6$ + NGF, and TCPS + NGF only got 74%, 70%, and 41% confluence, respectively. Finally, a notable difference was observed where NGF was used compared to the other conditions. In contrast to other experiments, NGF favors cell adhesion allowing the lowest migration results. By 70 hours, cell confluency reached 80% and 77% in (HEP/COL)6 + NGF and TCPS + NGF, respectively. These results are consistent with other researchers who have shown that the effects of NGF induce cell adhesion in hSCs.[15,16,18,38]

3.4.3 $(HEP/COL)_6$ stability studies from 0 to 30 days

3.4.3.1 Effect of the (HEP/COL)6 age on the hSCs viability

We prepared five microplates with $(HEP/COL)_6$ and pre-incubated them with cell medium during the periods established in **Table 3-1**. After each incubation period, the cell medium was removed, and the cells were seeded following the standard procedures for cell culture. Coating stability studies are carried out in relation to the hSCs response to $(HEP/COL)_6$ with different ages post-fabrication (0, 7, 14, 21, and 28 days). PrestoBlue™ cell viability reagent was used to determine the hSCs viability on $(HEP/COL)_6$ after three days of cell culture. The reducing environment of the cells modifies the structure of PrestoBlue, and it becomes a fluorescent molecule; therefore, by measuring the amount of fluorescence, we can also indirectly determine the number of living cell.[39]

Figure 3-5 shows the results of cell viability percentage for each microplate related to the manufacturing time of $(HEP/COL)_6$. As a first observation, Plate 1 cell cultures on $(HEP/COL)_6$ with and without NGF showed an increase in fluorescence intensity values close to 200%

compared to the TCPS control. Therefore, hSCs viability increases considerably under the culture conditions in which $(HEP/COL)_6$ was used. This result is consistent with our previous investigation, where for cultures after 6 days, we obtained an increase greater than 225% in cultures where $(HEP/COL)_6$ was used.[15] However, the favorable effects of $(HEP/COL)_6$ decrease as the hSCs are seeded on coatings with a longer fabrication time. Although in $(HEP/COL)_6$ of 14 and 21 days of manufacture, a slight increase in cell viability can still be observed, when culturing hSCs in 28-day coatings, the viability results were practically the same for all conditions, either TCPS or $(HEP/COL)_6$, which suggests that at this time there is an almost complete degradation of the multilayers. Cifuentes et al. characterized eight samples of HEP/COL multilayers deposited on flat silicon plates at 0- and 30-days post-fabrication. After analyzing the IR spectra, they demonstrated that in both types of samples, the relevant functional groups belonging to heparin and collagen were present in the wavelength range between 800 and 1700 cm^{-1} even after incubation for 30 days at ambient conditions (22°C and 40% relative humidity). Their results also showed that the 30-day samples showed very little change in peak intensity in comparison with same-day prepared samples.[35] For our case, $(HEP/COL)_6$ was incubated in parallel for 7, 14, 21, and 28 days with the Dulbecco's Modified Eagle's Medium. The incubation process was done by storage without shaking in an incubator (37°C and 5% CO_2). Almost complete $(HEP/COL)_6$ degradation at 28 days can be due to the action of the components of DMEM itself since it contains inorganic salts, such as NaCl, $CaCl_2$, or KCl; amino acids, and vitamins, among others.[40]

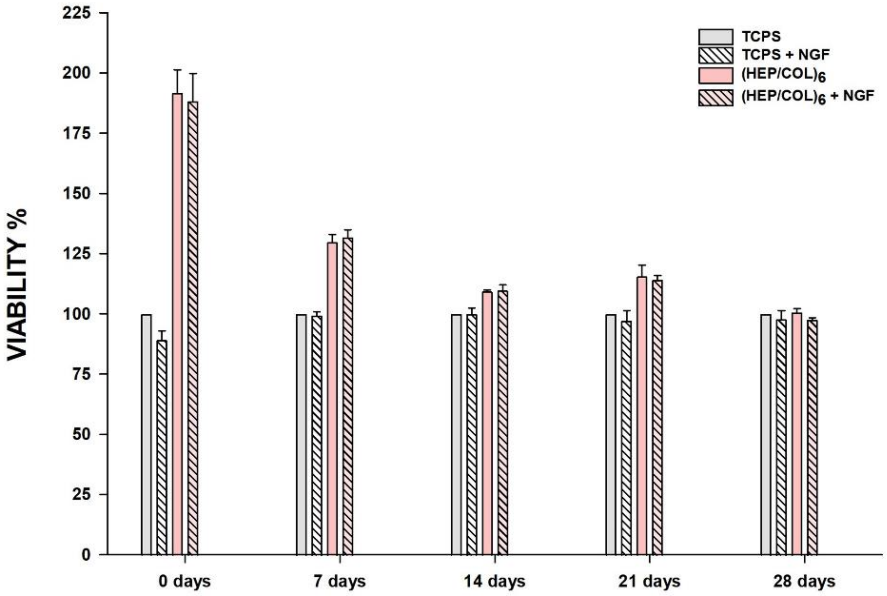

Figure 3-5. $(HEP/COL)_6$ stability assay showing hSCs viability after 3 days of cell culture on pre-incubated coatings. Before cell seeding, $(HEP/COL)_6$ was incubated during 0, 7, 14, 21, and 28 days with cell medium. Data are presented as the mean ± standard deviation of n = 5 samples.

3.4.3.2 Effect of the (HEP/COL)6 age on the hSCs real-time behavior

To investigate the real-time behavior of hSCs growth and adherence, we used the xCELLigence technology over $(HEP/COL)_6$ with different fabrication times. xCELLigence holds a system of biosensors that constantly measure bioelectrical impedance. The microsensors are in special microwell plates known as E-plates. Once the cells adhere to the bottom of the microwells, the system determines the resistance Z_i at a time *t*. Z_i values are compared with the initial background Z_0, which is measured using only culture medium solution.[41] This way, the number of adhered cells is translated into a special unit, the Cell Index (*CI*).[42,43] *CI* values are given by **Equation 1**:

$$\boldsymbol{CI = \frac{(Z_i - Z_0)}{15\Omega}} \qquad (\mathbf{1})$$

For this study, four plates were prepared with $(HEP/COL)_6$ and incubated with cell medium for 7, 14, 21, and 28 days before the hSCs were seeded. In **Figure 3-6**, cell index values are shown as a function of time for each plate. All the experiments were monitored for 80 hours. hSCs showed normal behavior for 80 hours on all plates, which is consistent with the results obtained in our previous investigation. Two regions attributed to cell adhesion and the proliferation phase were identified, between 0 to 30 hours and 30 to 80 hours, respectively.[15] This performance is independent of using $(HEP/COL)_6$ or its manufacturing time.

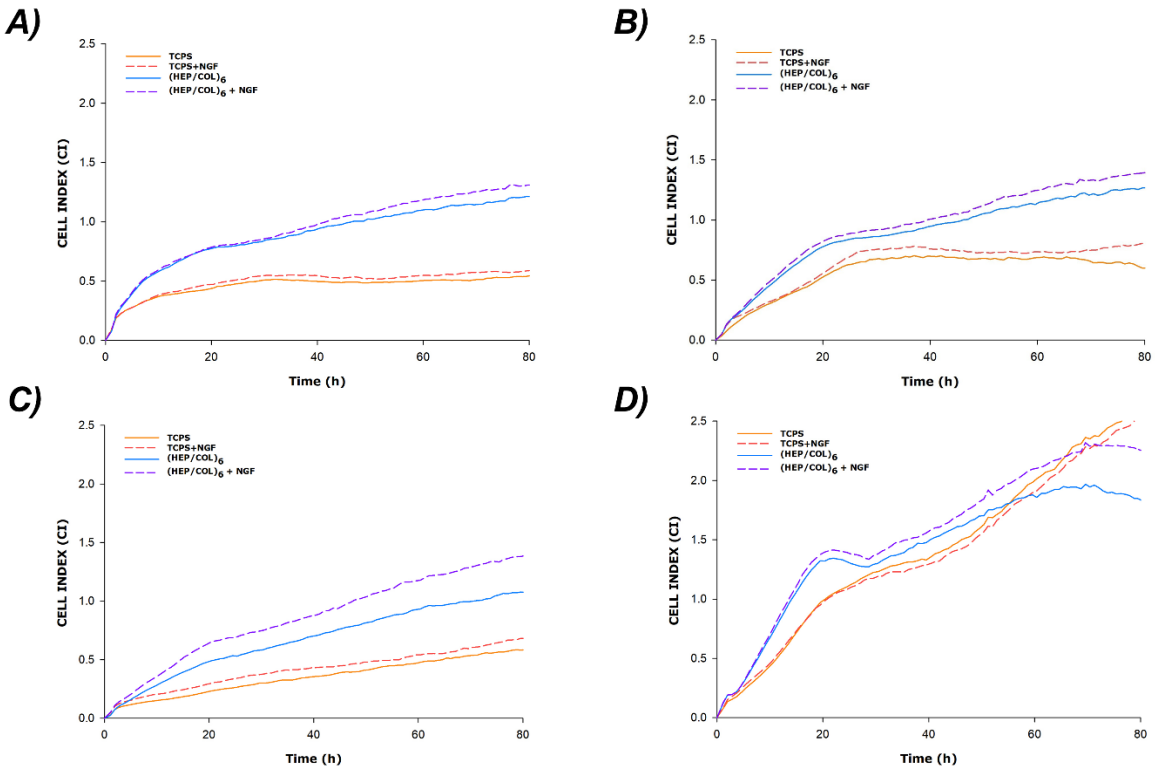

Figure 3-6. Real-time monitoring of hSCs behavior cultured for 80 hours in $(HEP/COL)_6$. Before cell seeding, $(HEP/COL)_6$ was previously incubated in cell culture medium for (A) 7, (B) 14, (C) 21, and (D) 28 days.

It is possible that initially $(HEP/COL)_6$ of 7 days post-fabrication is favored thanks to the coupling in the multilayers of some nutrients, vitamins, or other compounds from the culture medium (see

Figure 3-6A). However, **Figure 3-6** also showed how as we use coatings with a greater manufacturing time, the adhesion of the hSCs seeded on $(HEP/COL)_6$ tends to be more like that of the controls. This behavior can be seen when comparing **Figure 3-6A** and **Figure 3-6D**. The vast difference in cell adhesion initially found in 7-day coatings decreases considerably in 28-day plate, where the *CI* values for hSCs are almost the same. Again, this tendency suggests that with the increase of incubation days, the culture medium exerts a degrading effect on $(HEP/COL)_6$, and by 28 days, the multilayers may have completely reduced.

3.4.3.3 Cumulative heparin release from (HEP/COL)6 in cell medium and in PBS

Heparin release from $(HEP/COL)_6$ during contact tests with culture medium and PBS for 30 days is shown in **Figure 3-7**. Sampling in each well was performed every 72h. The manufacturing process of $(HEP/COL)_6$ involves the use of a washing step with a solution at pH=5; however, throughout the assay, no alteration in pH was observed in the culture medium, which would be indicated by a coloration change of the samples from red to orange. Whether the heparin release occurred towards the culture medium or PBS, a linear behavior was observed with a notable more significant effect exerted by the culture medium. Despite this linearity, it was possible to find a considerable difference in the average amount of heparin released in the different conditions, being 1.38 µg/day in culture medium against 1.12 µg/day in PBS, which represents a difference of 19% in the rate of dissolution for each day.

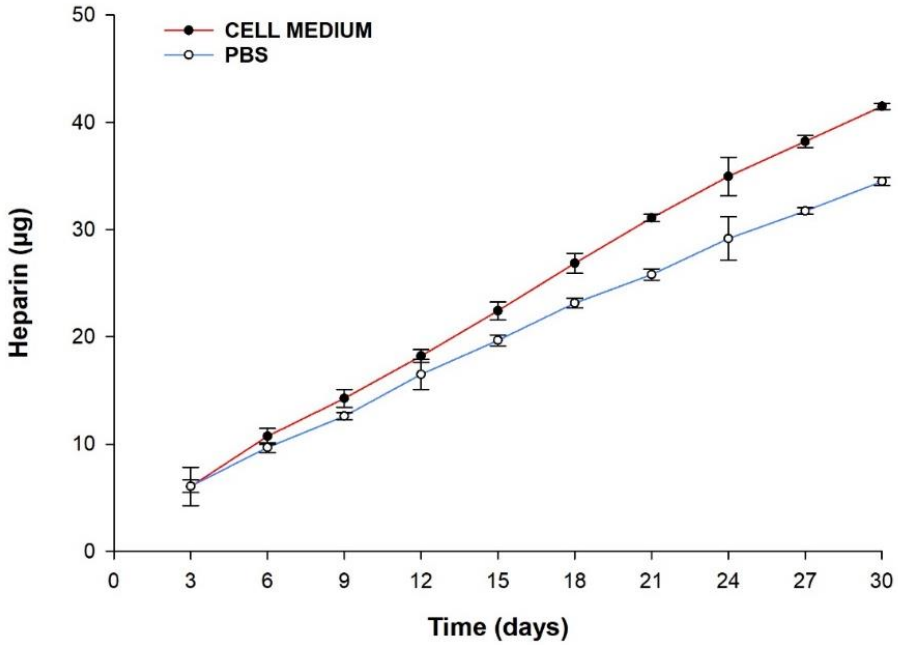

Figure 3-7. Heparin release from $(HEP/COL)_6$ in cell medium and in PBS. Sampling was performed every 72 hours from 3 to 30 days. Data are presented as the mean ± standard deviation of n = 8 samples.

3.4.4 Surface deposition of $(HEP/COL)_6$ on a commercial NGC

There is not much research on heparin/collagen coatings on NGCs. However, in this study we seek to demonstrate that using the traditional layer-by-layer dipping method, $(HEP/COL)_6$ could be deposited on NeuraGen®, a commercial collagen-based nerve guide conduit surface, as is shown in the representative approach in **Figure 3-8**.

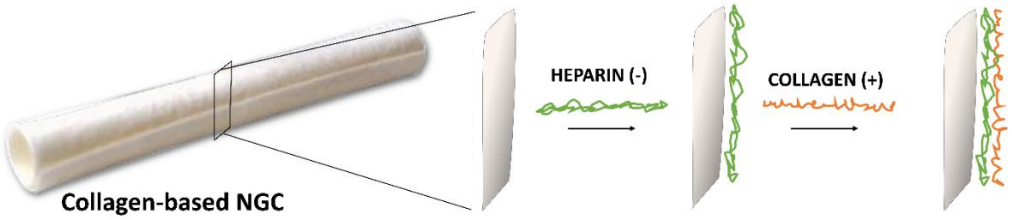

Figure 3-8. Approach for assembling of $(HEP/COL)_6$ on a collagen-based NGC.

$(HEP/COL)_6$ coated-NeuraGen® samples were analyzed with the Azure A dye colorimetric method to qualitatively determine the presence of heparin. The top of **Figure 3-9A** shows that mixing solid sodium heparin with Azure A solution turns the latter from blue to purple. When Azure A solution was applied to $(HEP/COL)_6$ coated-NeuraGen® samples (**Figure 3-9A** bottom), a change from blue to purple was also observed, which indicates the presence of heparin on the NGC surface. Assays or kits to detect collagen are expensive, and most require special conditions for their handling, involving some specific risks. Therefore, we consider that the positive colorimetric result with Azure A is sufficient evidence to demonstrate that the $(HEP/COL)_6$ deposition was performed over the NeuraGen® surface.

Finally, the structure of NeuraGen® is not affected by HEP/COL coatings, at least when 6 bilayers are deposited on its surface. Although the polymeric solutions have an acidic pH (close to 5), the morphology of the NGC was normal when compared to the control uncoated sample, and the formation of coatings on the fibers can be also evidenced (**Figure 3-9B**).

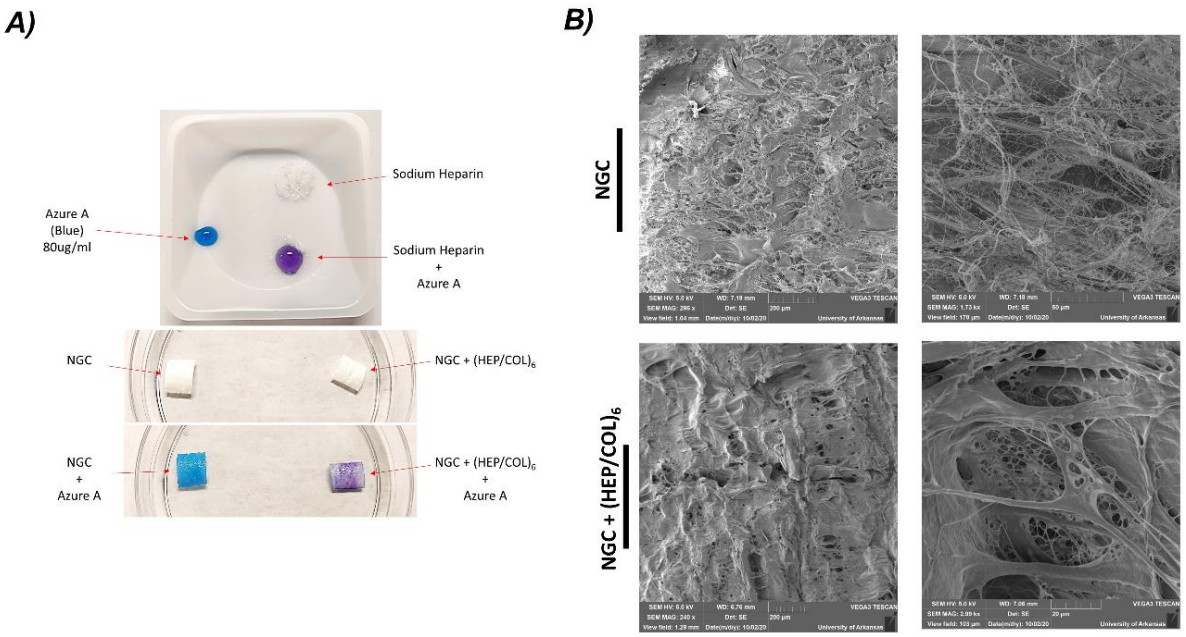

Figure 3-96. (A) Colorimetric detection of Heparin coatings on a commercial NGC with Azure A solution. Top: Azure A Solution (Blue) and Azure Solution A in the presence of Heparin (Purple). Center: Commercial NGC with and without $(HEP/COL)_6$ coatings. Bottom: Uncoated commercial NGC in the presence of Azure A (Blue) and $(HEP/COL)_6$ coated commercial NGC in the presence of Azure A (Purple); and (B) SEM images of uncoated commercial NGC (top) and $(HEP/COL)_6$ coated commercial NGC (bottom).

3.4.5 hSCs viability and adhesion on coated NGCs

Small circles of $(HEP/COL)_6$ coated and uncoated NeuraGen® samples were punched out with a diameter of 6 mm and placed in the bottom of wells of 96-well plates (working volume 200 µm). The samples were pretreated overnight by immersion in a culture medium solution. A high cell density of hSCs, 31,250 cells/cm^2, was allowed to grow for six days on the implants. After this time, the PrestoBlue reagent was used to measure cell viability. hSCs performance over coated NeuraGen® was similar to the results shown in **Sections 3.4.3.1** and **3.4.3.2** since $(HEP/COL)_6$ improved the cellular behavior concerning to the viability and adhesion. Uncoated samples were selected as the positive control, and their results were normalized to 100%. The effect of NGF added to the cell medium at 10ng/ml was also evaluated for this study. Uncoated NeuraGen® with NGF indicated a 25% increase in cell viability. At the same time, the conditions where NeuraGen®

was used with $(HEP/COL)_6$, with and without NGF, showed a more significant increase of 40% and 60%, respectively. Interestingly, the best results were achieved with $(HEP/COL)_6$ without NGF (**Figure 3-10B**). The effect of NGF in solution does not appear to increase viability significantly, as demonstrated in the TCPS assays.[15]

The fluorescence images evidenced cell adhesion, represented by blue nuclei, on both $(HEP/COL)_6$ coated and uncoated NeuraGen® samples (see **Figure 3-10A**).

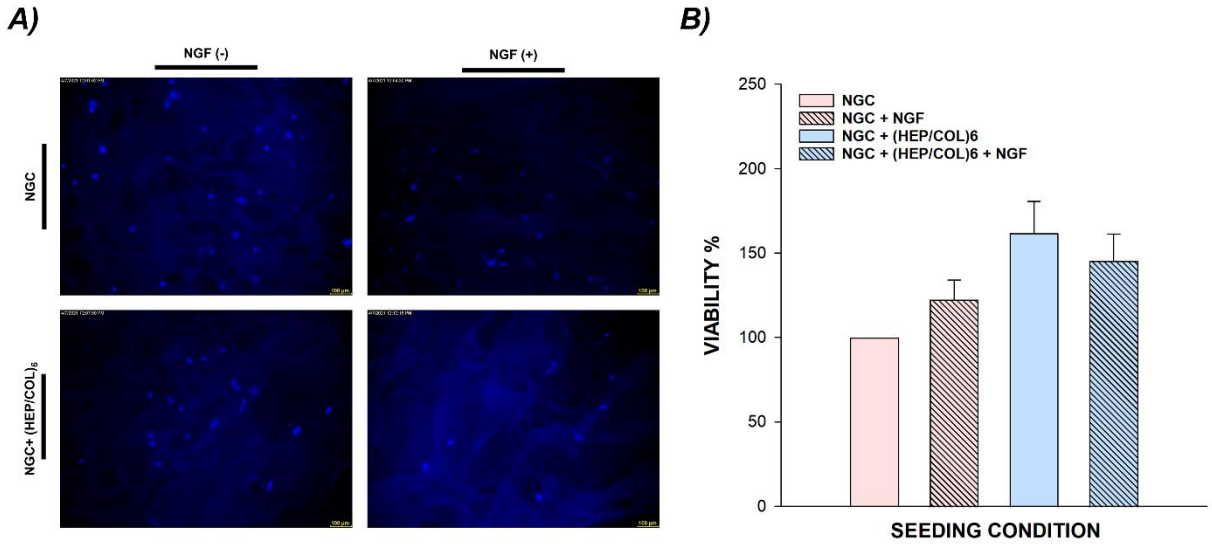

Figure 3-10. hSCs viability and adhesion on uncoated and $(HEP/COL)_6$ coated commercial NGCs. (A)Representative fluorescence microscopy image of hSCs nuclei labeled with Hoechst in cell cultures on uncoated and $(HEP/COL)_6$ coated commercial NGCs with and without NGF; and (B) PrestoBlue Viability assay for cultured hSCs on uncoated and $(HEP/COL)_6$ coated commercial NGCs with and without NGF after six days of culture.

3.5 Conclusions

The LbL technique can be efficiently applied to commercial collagen-based nerve guide conduit; therefore, we were able to modify NeuraGen® surface using $(HEP/COL)_6$. Our results showed that: (1) hSCs cultured in $(HEP/COL)_6$ showed an improved protein expression potential. (2)

$(HEP/COL)_6$ greatly promote hSCs migration, and the use of NGF exhibits an anti-migration effect. (3) $(HEP/COL)_6$ was stable up to 21 days after incubation with cell media before the cell seeding. The cell media exerts a strong action to degrade the coatings by 28 days post-fabrication and increasing the release of heparin in comparison with the effect of PBS. (4) Real-time monitoring also revealed a decrease in the enhancing potential of $(HEP/COL)_6$ when the coatings are exposed to cell media over time. (5) The morphology of NeuraGen® is not altered by the action of $(HEP/COL)_6$. And (6) An increase in the cell viability was observed in the condition where NeuraGen® with $(HEP/COL)_6$ was used.

3.6 Acknowledgment

Funding for this work was provided by the Arkansas Bioscience Institute. The authors thank Integra Life Sciences for their generous donation of lyophilized Type I Collagen and more than ten NeuraGen® samples used in this research. We also want to thanks to David Gonzalez-Nino, and Dr. Gary Prinz, for their support with SEM photos of the coated NGCs; and special thanks to the Northwest Arkansas Community College (NWACC) for his important participation in the 2022 REU program making possible the experiments for the stability studies.

3.7 References

[1] S.J. Bunn, CHARACTERIZATION OF SCHWANN CELLS STIMULATED BY DC ELECTRIC FIELDS, 2019.

[2] H. Jiang, Y. Qian, C. Fan, Y. Ouyang, Polymeric Guide Conduits for Peripheral Nerve Tissue Engineering, Front Bioeng Biotechnol. 8 (2020) 1–8. https://doi.org/10.3389/fbioe.2020.582646.

[3] L. Tian, M.P. Prabhakaran, S. Ramakrishna, Strategies for regeneration of components of nervous system: scaffolds, cells and biomolecules, Regen Biomater. 2 (2015) 31–45. https://doi.org/10.1093/rb/rbu017.

[4] K. Brattain, Analysis of the peripheral nerve repair market in the United States, (2013) 1–11. https://www.semanticscholar.org/paper/ANALYSIS-OF-THE-PERIPHERAL-NERVE-REPAIR-MARKET-IN-Brattain/cba129fbda15780ea0abd09da3da97de04f9c6b5 (accessed February 13, 2022).

[5] C.E. Schmidt, J.B. Leach, Neural Tissue Engineering: Strategies for Repair and Regeneration, Annu Rev Biomed Eng. 5 (2003) 293–347. https://doi.org/10.1146/annurev.bioeng.5.011303.120731.

[6] S. Madduri, B. Gander, Schwann cell delivery of neurotrophic factors for peripheral nerve regeneration, Journal of the Peripheral Nervous System. 15 (2010) 93–103. https://doi.org/10.1111/j.1529-8027.2010.00257.x.

[7] S. Ho, P. Labroo, K.M. Lin, S. Himanshu, J. Shea, B. Gale, J. Agarwal, Designing a Novel Drug Delivering Nerve Guide: A Preliminary Study, J Med Biol Eng. 39 (2019) 294–304. https://doi.org/10.1007/s40846-018-0393-y.

[8] B. Pfister, T. Gordon, J.R. Loverde, A.S. Kochar, S.E. Mackinnon, D.K. Cullen, Biomedical Engineering Strategies for Peripheral Nerve Repair: Surgical Applications, State of the Art, and Future Challenges, Crit Rev Biomed Eng. 39 (2011) 81–124. https://doi.org/10.1615/CritRevBiomedEng.v39.i2.20.

[9] C.A. Whittaker, K.F. Bergeron, J. Whittle, B.P. Brandhorst, R.D. Burke, R.O. Hynes, The echinoderm adhesome, Dev Biol. 300 (2006) 252–266. https://doi.org/10.1016/j.ydbio.2006.07.044.

[10] P. Arthur-Farraj, K.R. Jessen, Repair Schwann cell update: Adaptive reprogramming, EMT, and stemness in regenerating nerves, Glia. 67 (2019) 421–437. https://doi.org/10.1002/glia.23532.

[11] E. Mathey, P.J. Armanti, Introduction to the Schwann cell, in: P.J. Armanti (Ed.), The Biology of Schwann Cells: Development, Differentiation and Immunomodulation, Cambridge University Press, Cambridge, 2007: pp. 1–12. https://doi.org/10.1017/cbo9780511541605.

[12] R. Ayala-caminero, L. Pinzón-herrera, C.A. Rivera Martinez, J. Almodovar, Polymeric scaffolds for three-dimensional culture of nerve cells: a model of peripheral nerve regeneration, MRS Commun. 7 (2017) 391–415. https://doi.org/10.1557/mrc.2017.90.

[13] K. Zhang, D. Huang, Z. Yan, C. Wang, Heparin/collagen encapsulating nerve growth factor multilayers coated aligned PLLA nanofibrous scaffolds for nerve tissue engineering, J Biomed Mater Res A. 105A (2017) 1900–1910. https://doi.org/10.1002/jbm.a.36053.

[14] S.W.P. Kemp, A.A. Webb, S. Dhaliwal, S. Syed, S.K. Walsh, R. Midha, Dose and duration of nerve growth factor (NGF) administration determine the extent of behavioral recovery following peripheral nerve injury in the rat, Exp Neurol. 229 (2011) 460–470. https://doi.org/10.1016/j.expneurol.2011.03.017.

[15] L. Pinzon-Herrera, J. Mendez-Vega, A. Mulero-Russe, D.A. Castilla-Casadiego, J. Almodovar, Real-time monitoring of human Schwann cells on heparin-collagen coatings reveals enhanced adhesion and growth factor response, J Mater Chem B. 8 (2020) 8809–8819. https://doi.org/10.1039/d0tb01454k.

[16] S. Maniwa, A. Iwata, H. Hirata, M. Ochi, Effects of neurotrophic factors on chemokinesis of Schwann cells in culture, Scand J Plast Reconstr Surg Hand Surg. 37 (2003) 14–17. https://doi.org/10.1080/alp.37.1.14.17.

[17] Y. Uchida, M. Tomonaga, Nerve growth factor accelerates regeneration of cultured adult sympathetic ganglion cells, Age (Omaha). 8 (1985) 19–20. https://doi.org/10.1007/BF02431938.

[18] E.S. Anton, G. Weskampt, L.F. Reichardt, W.D. Matthew, Nerve growth factor and its low-affinity receptor promote Schwann cell migration, Proceedings of the National Academy of Sciences. 91 (1994) 2795–2799. https://doi.org/10.1073/pnas.91.7.2795.

[19] D.A. Castilla-Casadiego, L. Pinzon-Herrera, M. Perez-Perez, B.A. Quiñones-Colón, D. Suleiman, J. Almodovar, Simultaneous characterization of physical, chemical, and thermal properties of polymeric multilayers using infrared spectroscopic ellipsometry, Colloids and Surfaces A. 553 (2018) 155–168. https://doi.org/10.1016/j.colsurfa.2018.05.052.

[20] U. Warttinger, C. Giese, R. Krämer, Comparison of Heparin Red, Azure A and Toluidine Blue assays for direct quantification of heparins in human plasma, ArXiv. (2017) 1–15. https://doi.org/10.48550/arXiv.1712.03377.

[21] X. Li, FGFs in Injury Repair and Regeneration, in: Fibroblast Growth Factors, Elsevier, 2018: pp. 17–144. https://doi.org/10.1016/b978-0-12-816142-5.00002-3.

[22] Acro biosystems, Vascular endothelial growth factor -VEGF189, (n.d.). https://www.acrobiosystems.com/L-836-VEGF189.html?gclid=Cj0KCQjwjN-SBhCkARIsACsrBz5eX2Mv_thB8Men6BqhCeucDPt8IEXnrOwdI0bxxepZAJrw0UE6jF0aAndqEALw_wcB (accessed April 13, 2022).

[23] National Center for Biotechnology Information, HGF hepatocyte growth factor [Homo sapiens (human)], (n.d.). https://www.ncbi.nlm.nih.gov/gene?Db=gene&Cmd=ShowDetailView&TermToSearch=3082 (accessed March 31, 2022).

[24] J.K. Aronson, Meyler's Side Effects of Drugs: The International Encyclopedia of Adverse Drug Reactions and Interactions, 16th ed., Elsevier, Amsterdam, 2016.

[25] S.J. Cifuentes, P. Priyadarshani, D.A. Castilla-Casadiego, L.J. Mortensen, J. Almodóvar, M. Domenech, Heparin/collagen surface coatings modulate the growth, secretome, and morphology of human mesenchymal stromal cell response to interferon-gamma, J Biomed Mater Res A. 109 (2021) 951–965. https://doi.org/10.1002/jbm.a.37085.

[26] Abcam, Recombinant human TGF beta 1 protein (Active), (n.d.). https://www.abcam.com/recombinant-human-tgf-beta-1-protein-active-ab50036.html (accessed March 23, 2022).

[27] Santa Cruz Biotechnology, Anti-IL-8 Antibody (B-2): sc-8427, (n.d.). https://www.scbt.com/p/il-8-antibody-b-2?gclid=Cj0KCQjwjN-SBhCkARIsACsrBz7kq_PseWpq7oz3uwOQgl2ZwY-tnzmsUXjQ0F3_pvX0k6xMZXHMbKEaAvK2EALw_wcB (accessed April 7, 2022).

[28] Enzo Life Sciences, IL-10 (human), (recombinant), (n.d.). https://www.enzolifesciences.com/ENZ-PRT134/il-10-human-recombinant/ (accessed April 4, 2022).

[29] J. Xiao, A.W. Wong, M.M. Willingham, M. van den Buuse, T.J. Kilpatrick, S.S. Murray, Brain-derived neurotrophic factor promotes central nervous system myelination via a direct effect upon oligodendrocytes, Neurosignals. 18 (2011) 186–202. https://doi.org/10.1159/000323170.

[30] S. Fujiwara, S. Hoshikawa, T. Ueno, M. Hirata, T. Saito, T. Ikeda, H. Kawaguchi, K. Nakamura, S. Tanaka, T. Ogata, P. Kursula, SOX10 Transactivates S100B to suppress schwann cell proliferation and to promote myelination, PLoS One. 9 (2014). https://doi.org/10.1371/journal.pone.0115400.

[31] S.A. Stacker, M.G. Achen, Emerging roles for VEGF-D in human disease, Biomolecules. 8 (2018) 1–17. https://doi.org/10.3390/biom8010001.

[32] Santa Cruz Biotechnology, Anti-VEGF-D Antibody (C-12) sc-373866, (n.d.). https://www.scbt.com/p/vegf-d-antibody-c-12?gclid=Cj0KCQjwjN-SBhCkARIsACsrBz4T12EG-pdM_ygIPq4xCwS6DntZiEFzP5Gp4b_auYzZXVtgH4YqHh0aAtwbEALw_wcB (accessed April 13, 2022).

[33] J.R. Chan, T.A. Watkins, J.M. Cosgaya, C. Zhang, L. Chen, L.F. Reichardt, E.M. Shooter, B.A. Barres, NGF controls axonal receptivity to myelination by Schwann cells or oligodendrocytes, Neuron. 43 (2004) 183–191. https://doi.org/10.1016/j.neuron.2004.06.024.

[34] D. Cortés, O.A. Carballo-Molina, M.J. Castellanos-Montiel, I. Velasco, The non-survival effects of Glial cell line-derived neurotrophic factor on neural cells, Front Mol Neurosci. 10 (2017). https://doi.org/10.3389/fnmol.2017.00258.

[35] S.J. Cifuentes, P. Priyadarshani, D.A. Castilla-Casadiego, L.J. Mortensen, J. Almodóvar, M. Domenech, Heparin/collagen surface coatings modulate the growth, secretome, and morphology of human mesenchymal stromal cell response to interferon-gamma, J Biomed Mater Res A. 109 (2021) 951–965. https://doi.org/10.1002/jbm.a.37085.

[36] M. Piirsoo, A. Kaljas, K. Tamm, T. Timmusk, Expression of NGF and GDNF family members and their receptors during peripheral nerve development and differentiation of Schwann cells in vitro, Neurosci Lett. 469 (2010) 135–140. https://doi.org/10.1016/j.neulet.2009.11.060.

[37] P. Xu, K.M. Rosen, K. Hedstrom, O. Rey, S. Guha, C. Hart, G. Corfas, Nerve injury induces glial cell line-derived neurotrophic factor (GDNF) expression in schwann cells through purinergic signaling and the PKC-PKD pathway, Glia. 61 (2013) 1029–1040. https://doi.org/10.1002/glia.22491.

[38] H.M. Prentice, S.E. Moore, J.G. Dickson, P. Doherty, F.S. Walsh, M. Raff, Nerve growth factor-induced changes in neural cell adhesion molecule (N-CAM) in PC12 cells The effects of nerve growth factor (NGF) on the expression of neural cell adhesion molecule (N-CAM) in PC12 cells, 1987.

[39] Life Technologies Corporation, PrestoBlue™ Reagent Product Overview, Frequently Asked Questions. (2012) 1–13. https://assets.thermofisher.com/TFS-Assets/LSG/manuals/PrestoBlueFAQ.pdf (accessed July 7, 2020).

[40] Sigma-Aldrich Corporation, Dulbecco's Modified Eagle's Medium (DME) - Formulation, (n.d.). https://www.sigmaaldrich.com/deepweb/assets/sigmaaldrich/product/documents/441/501/d5648for.pdf (accessed November 19, 2022).

[41] J. Stefanowicz-Hajduk, A. Adamska, R. Bartoszewski, J.R. Ochocka, Reuse of E-plate cell sensor arrays in the xCELLigence real-time cell analyzer, Biotechniques. 61 (2016) 117–122. https://doi.org/10.2144/000114450.

[42] ACEA Biosciences Inc. USA, The xCELLigence system, (2013) 1–20. https://www.aceabio.com/wp-content/uploads/xCELLigence-RTCA-SP-MP-Instruments.pdf (accessed October 22, 2019).

[43] ACEA Biosciences Inc., xCELLigence ® RTCA S16 Operator's Manual, 2nd ed., ACEA Biosciences, Inc., San Diego, 2018.

CHAPTER 4. CONCLUSIONS AND FUTURE WORKS

4.1 Conclusions

This dissertation demonstrated that hSCs cultured over HEP/COL coatings showed improved growth compared to TCPS. An increase in cell number of up to 250% were evidenced in the cell cultures in where we use $(HEP/COL)_6$. Also, several properties of hSCs were also observed with an enhanced behavior:

- An advanced protein expression potential.
- An increase in the cell area over $(HEP/COL)_6$ with NGF.
- The real-time monitoring study revealed an enhancement in cell adhesion for the first phase in the cell growth.
- A non-altered morphology of hSCs in any of the culture conditions

Additionally, we could find that $(HEP/COL)_6$ greatly promote hSCs migration, the use of NGF exhibits an anti-migration effect and EdU assay revealed that $(HEP/COL)_6$ in combination with NGF slightly increases hSCs proliferation.

In relation to the characterization and stability of the coatings, by applying $(HEP/COL)_6$ to different substrates, we were able to determine the chemistry, surface charge, thickness, and morphology of coatings. $(HEP/COL)_6$ was stable up to 21 days after being incubated with cell medium solution prior to the cell seeding. Real-time monitoring also revealed a decrease in the enhancing potential of $(HEP/COL)_6$ when the coatings are exposed to cell media over time, and the heparin release experiment showed that cell media increases the release of heparin in comparison with the effect of PBS. We can conclude that cell media exerts a strong action to degrade the coatings by 28 days post-fabrication.

Finally, we were able to modify NeuraGen® surface using $(HEP/COL)_6$ and the morphology of NeuraGen® is not altered by the action of $(HEP/COL)_6$. As in TCPS tests, an increase in hSCs viability was reflected in the conditions where NeuraGen® with $(HEP/COL)_6$ was used.

4.2 Future works

Future studies of the (HEP/COL)6 effect on primary Schwann cells behavior are necessary. Because we would like to apply our coated NGCs in animal experimentation, initially with rats or mice, and we will seek to generate a PNI and use the implants as a repair treatment. Another critical study is the functionalization of GFs to the surface of NGCs. Within future minor studies, we will include:

- Perform a greater study of Protein Expression Potential using coated NGCs.
- Obtain SEM images of hSCs on coated NGCs.
- Study of the effect of the pH over the physical-chemical characteristics of (HEP/COL) multilayers.

APPENDIX

A.1 Supporting Information for Chapter 2

A preliminary qualitative test was carried out to determine the optimal initial cell concentration to be used in the experiments. Cells were seeded at 10,000, 40,000, 65,000, and 100,000 cells / cm^2 per well and confluence was observed after three days. Two culture conditions were compared: uncovered surfaces vs. $(HEP/COL)_6$. The results are shown in **Figure 2-S1** as fluorescence microscopy images.

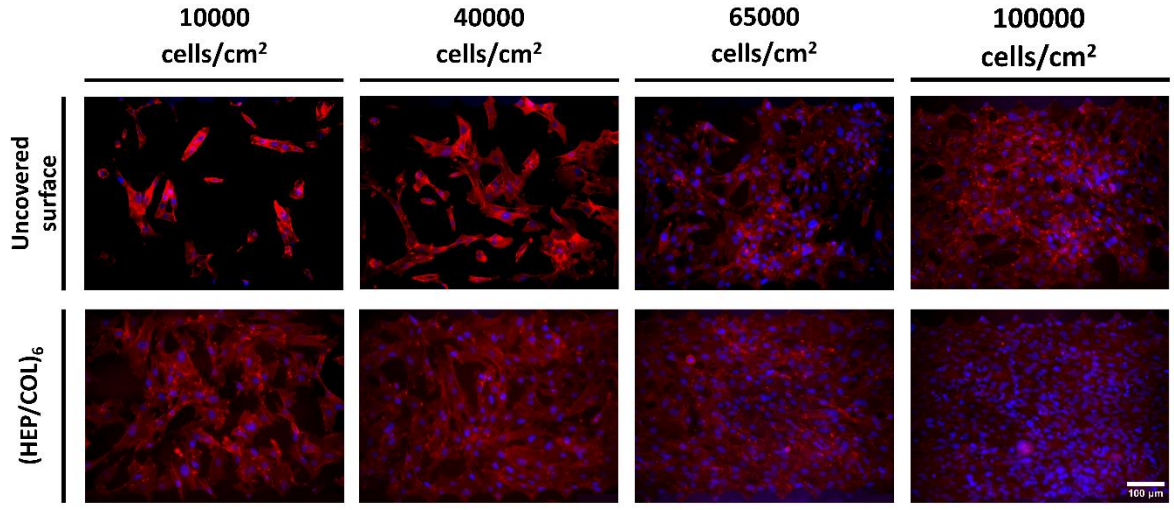

Figure 2-S1. Qualitative evaluation of the cell confluence after 3 days of culture according to the initial cell number. Representative fluorescence microscopic images of hSCs nuclei and actin labeled with Hoechst and Actin Red, respectively. Cellular behavior in cell cultures on uncoated surface and on $(HEP/COL)_6$.

The three most important stages of the colorimetric assay for the detection of Heparin using the Taylor's blue dye are shown in the **Figure 2-S2**. Coatings of 1, 2, 3, 4, 5, and 6 bilayers of HEP/COL were made on a 24-well plate. Once the bilayers were completely dry, the dye solution was added, which changes from blue to purple when interacting with Heparin. After the incubation period, the dye was removed, and the Heparin adhered to

the bottom of the well was observed to be stained purple. The last step is carried out by adding the dissociation reagent with a period of stirring to remove the Heparin from the bottom of the well. This step includes changing from colorless to light blue.

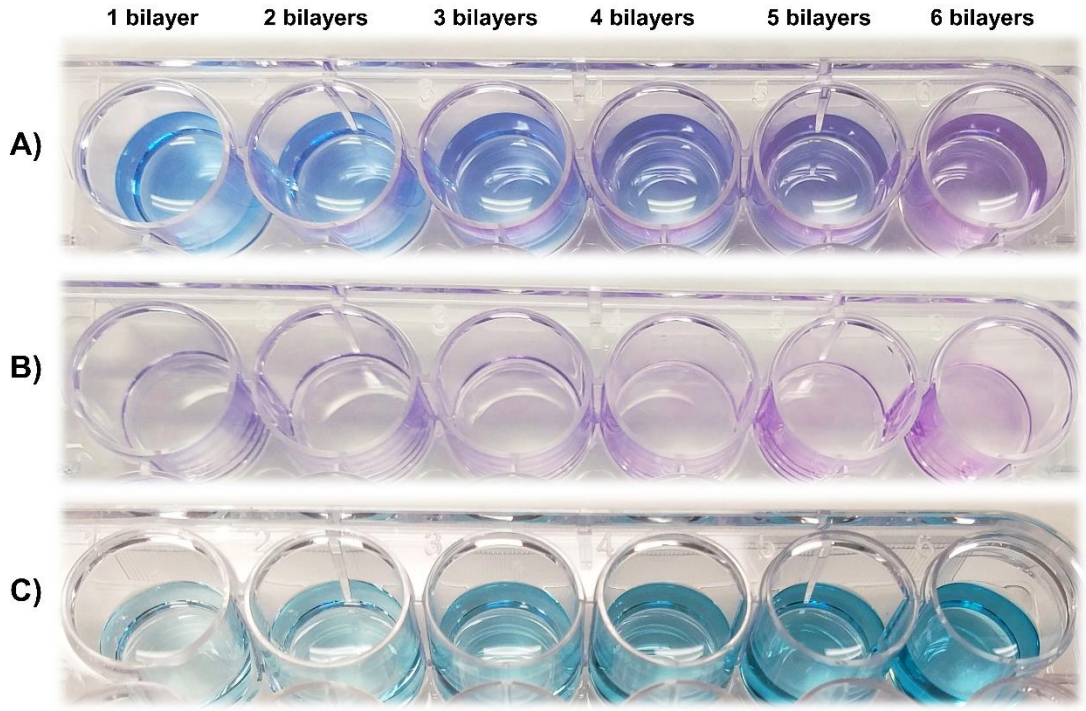

Figure 2-S2. Three main stages of the qualitative colorimetric assay for the detection of heparin with Taylor's blue dye. A) Incubation with Taylor's Blue dye (30 minutes), B) Dye adhered to Heparin (purple color at the bottom of the well) after removal of the solution, and C) Incubation with Dissociation Reagent with shaking for 10 minutes (change from colorless to light blue). The three images correspond to the same set of samples.

Figure 2-S3 shows the results for two experiments performed in which we analyzed the cellular behavior of hSCs in uncoated sensors with and without NGF added to the culture medium. An initial concentration of 20000 cells/cm^2 were seeded from our cell stock (passages No. 19 and 24). The Cell Index values were determined using the iCELLigence technology for 80 hours of cell culture.

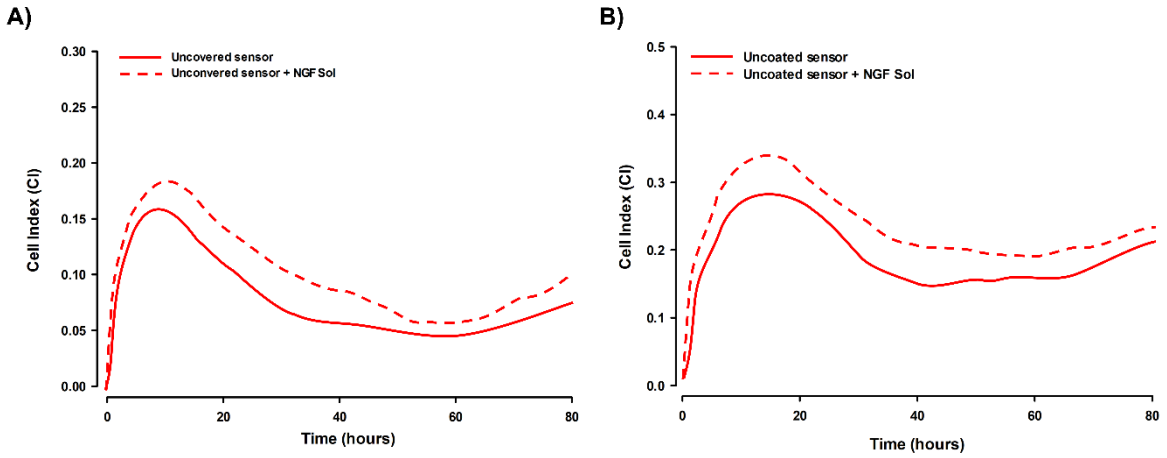

Figure 2-S3. Monitoring of real-time hSCs growth on uncoated sensors. Initial concentration of 20000 cells/cm^2 A) Experiment 1. Cellular behavior during 80 hours of cell culture, passage No. 24; and B) Experiment 2. Cellular behavior during 80 hours of cell culture, passage No. 19.